The petrology, geochronology and tectono-magmatic setting of igneous rocks in the Suckling-Dayman metamorphic core complex, Papua New Guinea

J.E. Ó¦sterle, T.A. Little, D. Seward, D.F. Stockli, J. Gamble

PII: S1342-937X(20)30066-6

DOI: https://doi.org/10.1016/j.gr.2020.01.014

Reference: GR 2300

To appear in: *Gondwana Research*

Received date: 3 October 2019

Revised date: 15 January 2020

Accepted date: 16 January 2020

Please cite this article as: J.E. Ó¦sterle, T.A. Little, D. Seward, et al., The petrology, geochronology and tectono-magmatic setting of igneous rocks in the Suckling-Dayman metamorphic core complex, Papua New Guinea, *Gondwana Research*(2020), https://doi.org/10.1016/j.gr.2020.01.014

The petrology, geochronology and tectono-magmatic setting of igneous rocks in the Suckling-Dayman metamorphic core complex, Papua New Guinea

Österle, J.E.[a,*)], Little, T.A. [a)], Seward, D.[a)], Stockli, D.F.[b)], Gamble, J.[a,c)]

[a)] School of Geography, Environment and Earth Sciences, Victoria University of Wellington, PO Box 600, Wellington, New Zealand.

[b)] Jackson School of Geosciences, The University of Texas at Austin, 2275 Speedway Stop C900, Austin, TX 78712-17221, USA.

[c)] School of Biological, Earth and Environmental Science, University College Cork, Cork, Ireland

Corresponding author: J.E. Österle – juergen.oesterle@email.com – +64 21 298 0995; School of Geography, Environment and Earth Sciences, Victoria University of Wellington, PO Box 600, Wellington, New Zealand

Abstract

Southeastern Papua New Guinea has hosted magmatism throughout the Cenozoic, with the latest phase being concurrent with active extension in the Woodlark Rift. There, the Suckling-Dayman metamorphic core complex (SDMCC) has exhumed middle-crustal rocks in the past few million years along a still-active low-angle normal fault, the Mai'iu Fault. Uplift of the SDMCC has exposed metasedimentary and metaigneous rocks of Late Cretaceous-Pleistocene age that record an evolution from oceanic spreading to subduction, to collision, and finally to subduction-inversion and extensional exhumation. We present new petrographic, whole-rock geochemical and geochronologic (outcrop and detrital zircon U–Pb) data from the SDMCC to reconstruct its long-term evolution. The dominant footwall-lithology of the SDMCC, the Goropu Metabasalt, has a MORB composition. Detrital zircons from metasedimentary beds intercalated with these basalts yield U–Pb-based maximum estimates for deposition of ~103 and ~72 Ma, suggesting a Late Cretaceous spreading age of the oceanic protolith. Bulk compositions of low-grade tholeiitic meta-gabbroic and -tonalitic rocks (Yau Igneous Complex) that intrude the Goropu Metabasalt reveal both enriched and depleted light rare earth element patterns. Zircon U–Pb ages from the Yau Igneous Complex range between ~60 and ~57 Ma, providing a minimum age for the formation of the Goropu Metabasalt. Much younger syn-extensional granitoids in the mafic footwall of the SDMCC have calc-alkaline to high-K compositions and U–Pb ages on zircon between ~3.7 and ~2.0 Ma. Our data indicate that the Mai'iu Fault had re-activated a Paleogene thrust as an extensional detachment fault by 3.7 ± 0.2 Ma. U–Pb ages of detrital zircons in modern streams draining the footwall of the SDMCC are essentially restricted to the

ages revealed by the Paleocene and Plio-Pleistocene intrusions. Xenocrystic zircons in the Plio-Pleistocene granitoids imply that the crust underlying the metabasaltic carapace of the SDMCC consists chiefly of Australian-continent derived sedimentary rocks.

Key words: Suckling-Dayman metamorphic core complex; zircon; U–Pb depth-profile dating; Southwest Pacific; Gondwana

1. Introduction

Southeastern Papua New Guinea (PNG) occupies the northern edge of the greater Australian continent (Fig. 1a) near the transition zone between the Tethyan and (proto-)Pacific tectonic domains (Zahirovic et al., 2016). The rock record of this region between the Southwest Pacific and Southeast Asia records a complex tectonic evolution since the Mesozoic breakup of Gondwana (Hill and Hall, 2003). New information on the tectonic history of this transitional domain can inform global paleogeographic reconstructions spanning the Tethyan and Pacific domains. Analysis and precise dating of igneous rocks of southeastern PNG can provide new clarity regarding the tectonic and geodynamic history of a region known to have featured multiple phases and loci of seafloor spreading (e.g., Coral Sea, Solomon Sea, Woodlark Basin, and perhaps the Pocklington Sea or Uyaknji Basin); and multiple phases and polarities of subduction and associated arc magmatism (Cape Vogel Arc, Melanesian Arc, Maramuni Arc; Davies et al., 1997; Dow, 1977; Gaina et al., 1999; Gaina and Müller, 2007; Holm et al., 2013, 2015, 2016, 2019; Jaques and Chappell, 1980; Rogerson et al., 1991; Walker and McDougall, 1982; Worthing and Crawford, 1996).

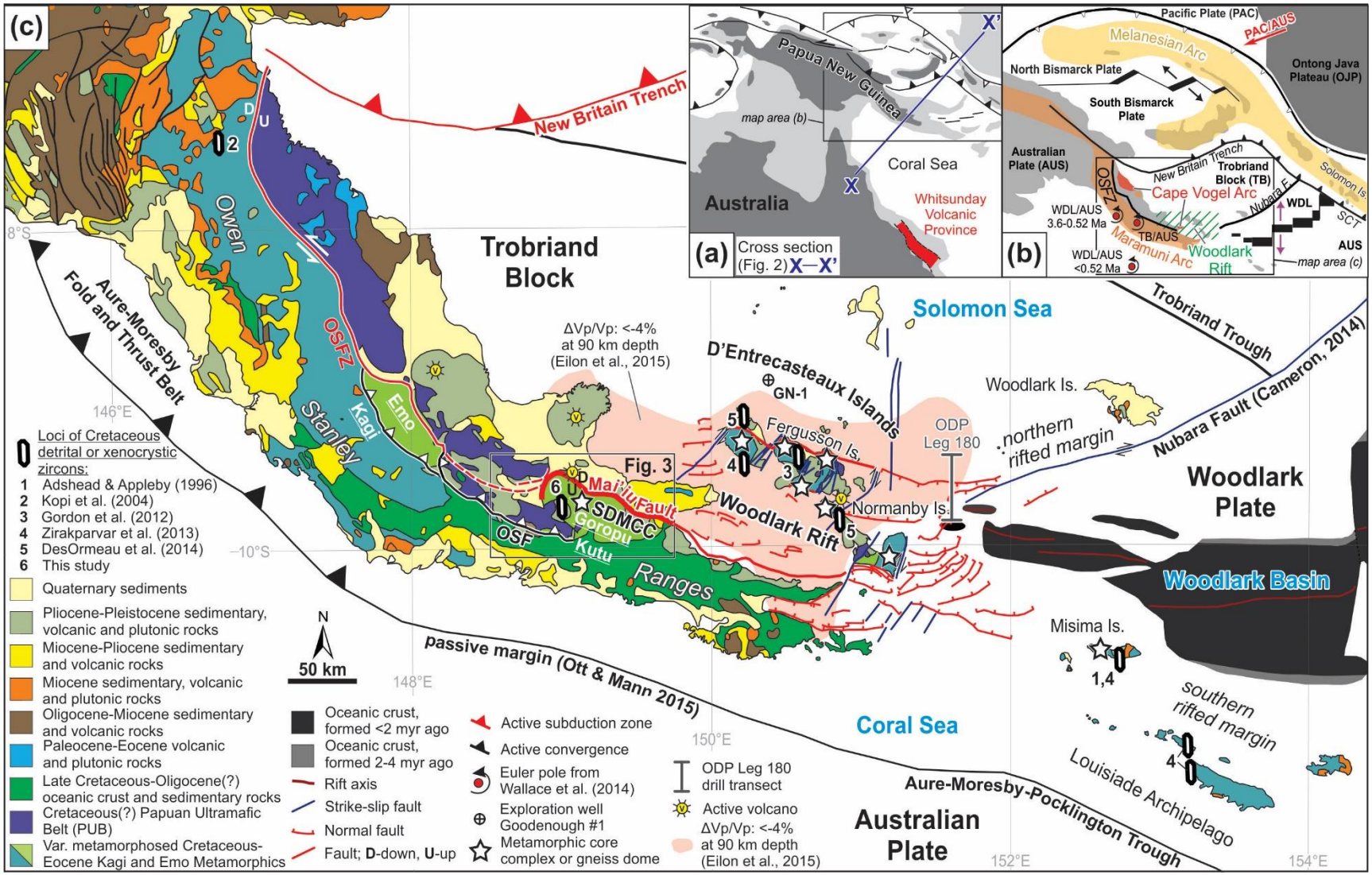

Fig. 1. (a) Inset map: Contemporary plate tectonic map of the Australia-PNG region modified from Hall (2002) and Webb et al. (2014). Dark and light gray areas represent landmass and continental shelves at the 200-m isobath, respectively. (b) Inset map: Contemporary plate tectonic map of southeastern PNG modified from Wallace et al. (2004, 2014) after Baldwin et al. (2012) and Holm et al. (2019). Abbreviations: OSFZ – Owen Stanley Fault Zone, SCT – San Cristobal Trench, WDK – Woodlark Plate. Red bold arrow (PAC/AUS) represents contemporary velocity of the Pacific Plate relative to the Australian Plate (10-11 cm/yr). Small purple arrows represent Woodlark-Australia spreading in the Woodlark Basin. (c) Simplified geological map of southeastern PNG modified from D'Addario et al. (1976) after Baldwin et al. (2004), Cameron (2014), Ott and Mann (2015), Abers et al. (2016) and Little et al. (2019). Abbreviations: Emo – Emo Metamorphics, Goropu – Goropu Metabasalt, Kagi – Kagi Metamorphics, Kutu – Kutu Volcanics, OSF – Owen Stanley Fault, OSFZ – Owen Stanley Fault Zone, SDMCC – Suckling-Dayman metamorphic core complex. Extent of mantle V_p anomaly at 90 km depth is from Eilon et al. (2015). Location of active volcanoes from Davies and Smith (1971). Location of ODP Leg 180 drill hole transect from Taylor and Huchon (2002). Note, the black line labelled OSF and the one separating the Kagi Metamorphics from the Emo Metamorphics (secondary thrust) represent preserved thrust faults. Where the OSF has been reactivated in the Neogene, it is termed the OSFZ (red solid line, approximately 147°E to 148°E) and marks the active plate boundary (Australian Plate vs. Trobriand Block) based on geologic, geomorphic and geodetic observations (e.g., Dow, 1977; Wallace et al., 2004; 2014). Farther to the southeast, the OSF was reactivated as the Mai'iu Fault (red solid line, bounding the SDMCC to the north).

The nature, petrogenesis and timing of magmatism in this remote and difficult-to-study region remain poorly resolved. Reconnaissance work and mapping in southeastern PNG undertaken by the Bureau of Mineral Resources of Australia and the Geological Survey of Papua New Guinea in the 1960s and 1970s (e.g., Davies and Smith, 1974; Dow et al., 1974; Pieters, 1978; Smith and Davies, 1976) in many areas remains the only geological knowledge available. Understanding of the region has also been hindered by most previous geochronology of the igneous rocks of the Papuan Peninsula having relied on either K–Ar dating (e.g., Davies and Smith, 1974; Dow et al., 1974; Pieters, 1978; Rogerson et al., 1991; Rogerson and Hilyard, 1989)—which is blind to non-closed system behavior of Ar in the host phase (e.g., incorporation of excess Ar); or on fossil ages (e.g., Belford, 1976), which are not always precise. Lastly, many previously published geochemical datasets for this region report no (or only limited) analyses of trace elements (e.g., Ruxton, 1966; Smith, 1972; Smith and Davies, 1976), making compositional-based comparisons between the rock units difficult and restricted to major oxide data or even petrographic observations.

Our study focuses on the plutonic rocks exposed in the Suckling-Dayman metamorphic core complex (SDMCC). The bounding Mai'iu Fault has exhumed in its footwall a mid-crustal section containing metasedimentary and metaigneous rocks that document the remarkable tectonic history of this metamorphic core complex (MCC). These rapidly exhumed rocks include some of the youngest known granitoids on Earth (e.g., Ito et al., 2017; Sano et al., 2002). We present the first outcrop zircon U–Pb LA-ICP-MS ages for the Suckling Granite, Mai'iu Monzonite,

Bonua Porphyry—previous sparse K–Ar and U–Pb ages from these units were determined on stream boulders—and the Yau Igneous Complex, integrated with whole-rock major oxide and trace element geochemistry. Moreover, detrital zircon U–Pb ages allow us to date the seafloor spreading that created the MORB-composition Goropu Metabasalt in a marginal basin to the northeast of continental Australia. Lastly, detrital zircon U–Pb analyses of modern stream sediments allow us to characterize rainforest-covered catchments in the footwall of the SDMCC that are otherwise inaccessible, thereby increasing the spatial coverage of our study. Our age constraints provide a temporal baseline for the tectonic evolution of this part of the Southwest Pacific region, a history that ultimately led to the formation and exhumation of the SDMCC in the Woodlark Rift.

1.1 Tectonic framework

Today, PNG is situated in a tectonically complex plate boundary zone between the Pacific and Australian Plates (Fig. 1b). This plate boundary zone consists of several rotating microplates that accommodate the rapid oblique convergence (110 mm/yr) of the approaching Pacific and Australian Plates through convergent, transform and divergent plate boundary processes (Koulali et al., 2015; Tregoning et al., 1998; Wallace et al., 2004). In southeastern PNG, active deformation is accommodated by rifting and seafloor spreading of the Woodlark system.

The SDMCC is the westernmost of a series of MCCs and extensional gneiss domes in the active Woodlark Rift (Fig. 1c) that also includes the D'Entrecasteaux Islands and Misima Island (Abers et al., 2016; Baldwin et al., 2008; Daczko et al., 2009, 2011; Davies, 1980; Davies and Warren, 1988; Little et al., 2007, 2019; Peters, 2007; Webb et al., 2008). The footwall of the SDMCC is currently being exhumed along the Mai'iu Fault (Fig. 1c)—an inverted subduction thrust that is part of the Owen Stanley Fault system (Davies, 1980; Little et al., 2019). Today, the Mai'iu Fault forms the plate boundary between the Australian Plate, to the south, and the Trobriand Block-Solomon Sea, to the north (Figs. 1b and c; Wallace et al., 2004, 2014). Counter-clockwise rotation of the Trobriand Block and neighboring Woodlark Plate relative to the Australian Plate about nearby Euler poles since the Late Miocene has resulted in extension of the continental Woodlark Rift, to the west; and seafloor spreading in the Woodlark Basin to the east (Fig. 1c)—processes that continue today (Taylor et al., 1999; Wallace et al., 2014).

The age of inception of Woodlark rifting is still debated and poorly resolved (Petersen and Buck, 2015; Taylor and Huchon, 2002; Webb et al., 2014). Even less clear are the role and configuration of older tectonic elements dating back to the Cretaceous in this region (Holm et al., 2016, 2019; Smith, 2013; Whattam, 2009). One of the most contentious of these is the Trobriand Trough (Fig. 1c; Abers and Roecker, 1991; Cooper and Taylor, 1987; Davies et al., 1984). Combining available geological and geophysical datasets into a plate tectonic model, Holm et al. (2016) inferred that the Trobriand Trough was a short-lived subduction zone that initiated at ~6 Ma and started slowing at ~2 Ma. If so, a lack of seismicity suggests that the

Trobriand Trough is not active as a subduction zone today (Abers and Roecker, 1991; Abers et al., 2016).

There is also debate about the identity and polarity of the subduction zone that carried Late Cretaceous, Australian margin-derived mafic and felsic rocks, now exposed in the gneiss domes of the D'Entrecasteaux Islands, to eclogite-facies conditions (Davies and Warren, 1988; Little et al., 2019; Petersen and Buck, 2015; Webb et al., 2014; Zirakparvar et al., 2013). The Late Miocene-Early Pliocene aged high pressure to ultra-high pressure (HP-UHP) metamorphism may have been a consequence of northward subduction of the Australian margin at either a) the Aure-Moresby-Pocklington Trough (Webb et al., 2014); or b) an unmapped subduction zone to the north of the current D'Entrecasteaux Islands (Petersen and Buck, 2015); or c) an in part exposed subduction zone that lies structurally below the Goropu Metabasalt in the footwall of the SDMCC (Little et al., 2019). Little et al. (2019) place the north-dipping subduction thrust at the contact between the Kagi Metamorphics and the structurally overlying Goropu Metabasalt near the SDMCC, the latter of which are considered laterally equivalent of the Emo Metamorphics on the Papuan Peninsula farther to the northwest (Fig. 1c) based on their similar structural position, rock type and metamorphic grade (Davies and Jaques, 1984; Pieters, 1978; Worthing and Crawford, 1996).

1.2 Magmatism in southeastern PNG and its tectonic setting

The evolution of the Papuan Peninsula likely began in the Early Cretaceous along the northeastern margin of Australia, then situated at the northeastern edge of Gondwana (Hill and Hall, 2003). Erosion of the Australian continent and widespread Aptian-Cenomanian volcanism along its northern and eastern margins (e.g., Dow, 1977; Dow et al., 1972; Hill and Gleadow, 1990; Hill and Hall, 2003) led to the accumulation of a ≥10-km thick volcano-sedimentary sequence atop rifted continental crust of the Australian Plate (Bulois et al., 2017). This sequence included the Whitsunday Volcanic Province in present-day Queensland, Australia (Bryan et al., 1997; Ewart et al., 1992), and the lithologically similar Kagi Metamorphics (Pieters, 1978) in what is now the Papuan Peninsula in PNG (Figs. 1a and c).

Southwest-directed subduction of the Pacific Plate beneath the early Melanesian Arc (*sensu lato*) in the Cretaceous (Tapster et al., 2014) led to back-arc spreading between the latter and the Australian continent (Figs. 1b and 2). A probable element of this back-arc basin system is the Emo back-arc basin (Whattam, 2009; Worthing and Crawford, 1996) or the Emo Basin (Seton et al., 2016; Figs. 2 and S2). The inferred remnants of this oceanic basin consist of lawsonite-actinolite to greenschist-facies tholeiitic basic schists, the Emo Metamorphics (Fig. 1c; Pieters, 1978). The suggested age of the Emo Metamorphics, Maastrichtian, has been based on the identification of planktonic foraminifera in metasedimentary beds (the Bonenau Schist) that are locally intercalated with the inferred lateral equivalent of the former, the Goropu Metabasalt (Fig. 1c), which forms much of the footwall of the SDMCC (Pieters, 1978; Smith and Davies, 1976). Which of several other similarly mafic units (Brown, 1977; Macnab, 1969; Nion et al., 1987; Rogerson et al., 1986; Smith, 2013; Wai et al., 1994) that are exposed semi-continuously along the

southwestern flank of the Owen Stanley Ranges (Figs. S1 and S2) should also be considered as part of this back-arc basin assemblage is unclear because of a lack of reliable age and sparse geochemical data. In New Caledonia, rocks of the Poya Terrane (Cluzel et al., 2001) show striking similarities to the above-mentioned mafic rocks on the Papuan Peninsula in terms of age, composition and tectonic history (see section 4.1), suggesting a similar origin of both regions.

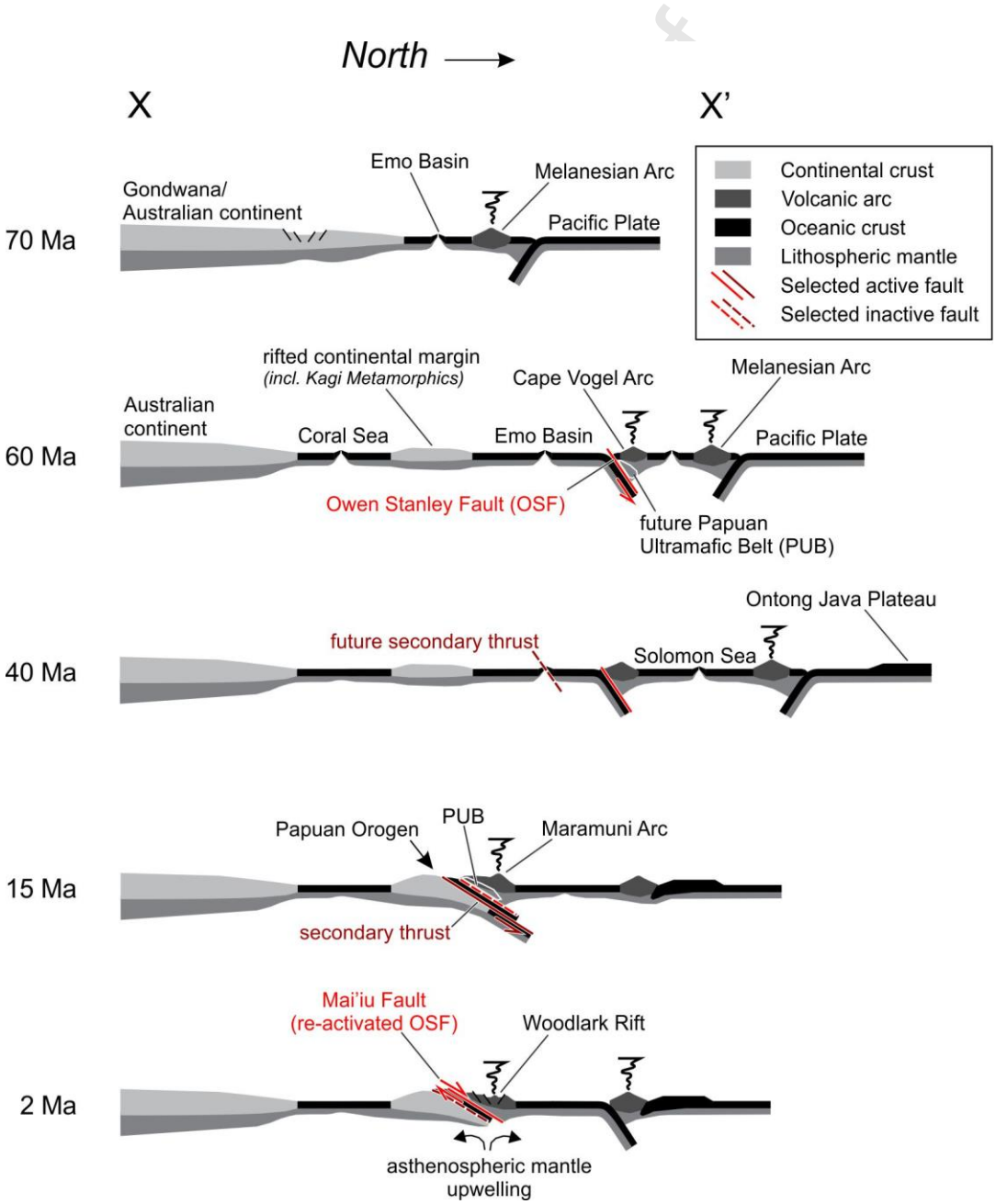

Fig. 2: Schematic tectonic reconstruction of the southeastern Papuan New Guinea region along cross-section line X-X' (for location see Fig. 1a) with a fixed Australian continent reference frame modified from previous reconstructions of Holm et al. (2013), Little et al. (2019), Tapster et al. (2014) and Whattam (2009).

In the Paleogene, the Owen Stanley Fault accommodated north-eastward subduction of the Emo Basin beneath an island arc terrane known as the Cape Vogel (or Dabi) Arc (CVA; Figs. 1b and 2; Glen and Meffre, 2009). This contractional regime was contemporaneous with opening of the Coral Sea (62-52 Ma; Gaina et al., 1999) between the Australian continent, to the south, and other rifted continental crust (the submerged Eastern and Papuan Plateaus south of the Papuan Peninsula, not shown), to the north. Exposed submarine tholeiitic and boninite lavas, andesitic-rhyolitic volcaniclastics and diorite-tonalite intrusions (Figs. S1 and S2) suggest that the CVA was active in the Paleocene-Eocene (~59-47 Ma; Jaques and Chappell, 1980; Rogerson et al., 1991; Walker and McDougall, 1982). Subduction of the oceanic Emo Basin beneath the CVA later transitioned to collision when the northern Australian rifted margin, including its volcanogenic sedimentary cover (the Kagi Metamorphics), jammed the subduction channel (Davies and Jaques, 1984). During this collision, the CVA and its fore-arc basement, the Papuan Ultramafic Belt (PUB, Fig. 1), were thrust south-westward over the distal Australian continental margin (Fig. 2; Davies and Jaques, 1984). The resultant Papuan Orogen (or Peninsular Orogen, van Ufford and Cloos, 2005) occupies the mountainous spine of the Papuan Peninsula, the Owen Stanley Ranges. $^{40}Ar/^{39}Ar$ plateau ages for metamorphic

hornblende from the sole of the PUB suggest that obduction of the arc basement had begun by 58.3 ± 0.4 Ma (Lus et al., 2004).

To the north of the CVA, subduction of the Pacific Plate beneath the Melanesian Arc ceased when the Ontong Java Plateau (Fig. 2) arrived at the subduction zone at ~26 Ma (Holm et al., 2013; Knesel et al. 2008). In the rear of this subduction zone, the Solomon Sea had opened during the Paleogene between the Cape Vogel and Melanesian Arcs. The timing of the opening is still debated (Davies and Jaques, 1984; Falvey and Pritchard, 1982; Joshima et al., 1986; Joshima and Honza, 1986), but preserved chrons 19-15 suggest a Middle to Late Eocene (45-35 Ma) age (Gaina and Müller, 2007).

In the Middle-Late Miocene, PNG was the site of widespread calc-alkaline to shoshonitic magmatic activity of the Maramuni Arc (Baldwin et al., 2012; Dow, 1977; Page, 1976). Miocene igneous rocks with arc-like geochemical affinities are encountered along the length of the Papuan Peninsula, in the Woodlark Rift and the northern and southern rifted margins of the Woodlark Basin (Baldwin et al., 2012; Figs. S1 and S2). This magmatism has been attributed by some to southward underthrusting of the oceanic Solomon Sea crust at the Trobriand Trough (Cooper and Taylor, 1987; Davies et al., 1984; Francis et al., 1987), and by others to north-directed subduction of a cryptic Jurassic-Cretaceous oceanic basin (Pocklington Sea; Holm et al., 2015) or Australian rifted margin (Webb et al., 2014) at the Aure-Moresby-Pocklington Trough. Which igneous units in southeastern PNG constitute the Maramuni Arc is, however, controversial. For example, Webb et al. (2014) attributed a ~12 Ma hornblende $^{40}Ar/^{39}Ar$ plateau age from a dacite sill of the

Panarora Volcanics (Figs. S1 and S2) in metasedimentary rocks on the Louisiade Archipelago—akin to those of the Kagi Metamorphics on the Papuan Peninsula—to mark the initial stages of Woodlark rifting rather than activity of the Maramuni Arc.

In the Woodlark Basin, magnetic data indicate that seafloor spreading in the basin had initiated by ~6 Ma (Taylor et al., 1999); however, the timing of onset of continental rifting farther to the west is uncertain. The rifting onset has been estimated at ~12 Ma based on the occurrence of the above-cited dacite sill cross-cutting an accretionary complex attributed to a Miocene-age, north-dipping subduction zone – the trench of which is marked by the Aure-Moresby-Pocklington Trough – by Webb et al. (2014). Alternatively, an onset age of ~8.4 Ma is suggested on the basis of regional stratigraphic arguments by Taylor and Huchon (2002); whereas Petersen and Buck (2015) used finite extension arguments to infer an onset age of ~4 Ma. An extensive record of latest Miocene-Recent volcanic and plutonic rocks that fall within the temporal and spatial reaches of the Woodlark Rift are preserved on the southeastern Papuan Peninsula (as far east as 148°E), the D'Entrecasteaux Islands and the Egum Atoll (Figs. S1 and S2). Despite the patently extensional present-day tectonic regime, most of these igneous rocks have arc-like geochemical signatures. Only in the Dawson Strait between Fergusson and Normanby Islands are peralkaline rhyolites of the Quaternary Dawson Strait Volcanics (Figs. S1 and S2) unambiguously attributed to the extensional tectonics of the Woodlark Rift (Smith, 1976; Smith et al., 1977). Farther south on the southwest coast of the Papuan Peninsula, however, the tectonic origin of late Middle Miocene-Pliocene volcanic rocks (Figs. S1 and S2) remains uncertain (Holm and Poke, 2018).

1.3 The Suckling-Dayman metamorphic core complex

In the western Woodlark Rift, extension on the active and rapidly slipping Mai'iu Fault has exhumed an up to ~3.7-km-high, ~60-km-long, east-west-elongate topographic dome during the past few million years (Daczko et al., 2009, 2011; Davies, 1980; Little et al., 2019)—the SDMCC (Fig. 3). Three summits (Mts. Suckling, Dayman and Masasoru; Fig. 3) are built on ~20-40-km-spaced antiformal culminations in the corrugated footwall of that MCC (Daczko et al., 2011; Little et al., 2019). This extensionally exhumed footwall consists chiefly of a ~3-4-km-thick carapace of low-grade metabasalt (Goropu Metabasalt) of MORB affinity (Davies, 1980; Smith, 2013). The thickness of this unit is inferred by its correlation to the similarly basaltic, but less metamorphosed, Kutu Volcanics that crop out to the south of the SDMCC. The Goropu Metabasalt includes subordinate hyaloclastite, pelagic limestone, tuffaceous marl and calcareous-siliceous phyllite (Davies, 1980; Davies and Smith, 1974). Locally, deformed pillow structures are preserved in the Goropu Metabasalt (Smith and Davies, 1976).

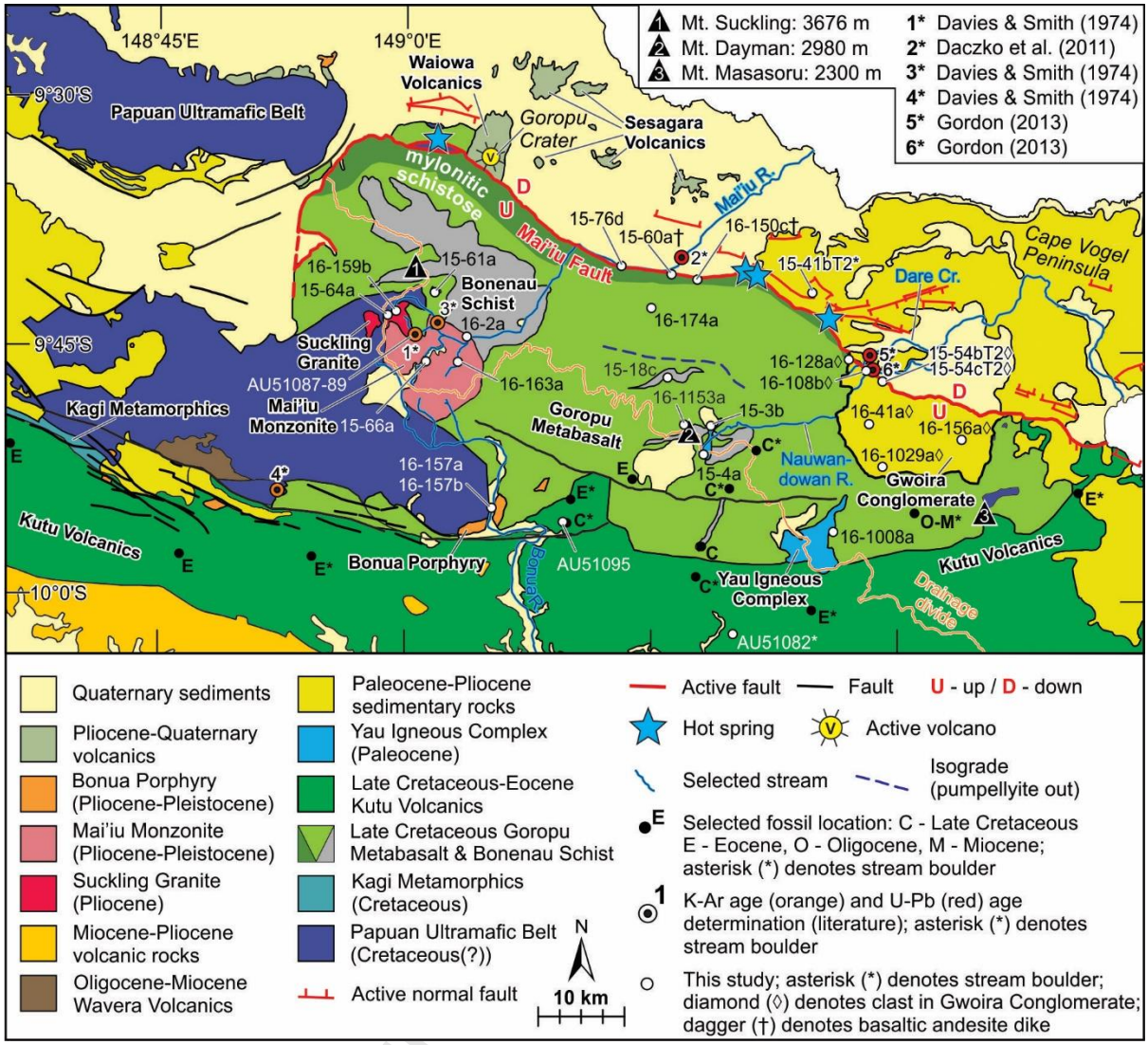

Fig. 3: Geological map of the Suckling-Dayman metamorphic core complex. Modified from Davies and Smith (1974), Lindley (2014) and Little et al. (2019). Location of zircon U–Pb age samples from Caffi (2008) and Gordon (2013).

The metamorphic grade in the Goropu Metabasalt decreases southward from greenschist facies near the Mai'iu Fault in the north, to pumpellyite-actinolite facies on the northern flank of the SDMCC, to prehnite-pumpellyite facies south of its crest. Still farther to the south, it grades into unmetamorphosed basalts of the Kutu Volcanics (Davies, 1980; Smith, 2013; Smith and Davies, 1976). The age of these

metamorphosed (Goropu Metabasalt) and unmetamorphosed (Kutu Volcanics) basalts are constrained by Late Cretaceous (Maastrichtian) and Eocene planktonic foraminifera (12 samples in the map area, Fig. 3) of (meta)sedimentary rocks that are interbedded with the volcanic rocks, and also in stream boulders derived from them (Smith and Davies, 1976). At one other locality, fossils in a stream boulder in an area mapped as Goropu Metabasalt (Fig. 3) are reported to be as young as Oligocene-Early Miocene (Smith and Davies, 1976). Interbeds in the unmetamorphosed Kutu Volcanics to the south mostly contain Eocene planktonic (and rare benthonic) foraminifera (Smith and Davies, 1976). Near Mts. Suckling and Masasoru, the Goropu Metabasalt is structurally overlain by deformed ultramafic and gabbroic rocks of the PUB (Fig. 3; Davies, 1980). This contact is inferred to be a remnant of the Owen Stanley Fault (Davies, 1980; Little et al., 2019). Although the surface geology of the footwall of the SDMCC and its surroundings is dominantly mafic-ultramafic in composition (Davies and Smith, 1974; Smith and Davies, 1973a, 1973b), seismic studies (Abers et al., 2016; Ferris et al., 2006; Jin et al., 2015) indicate that the underlying crust is 30-40 km thick and of bulk intermediate-felsic composition (V_P = 5.6-6.9 km/s at 10-25 km depth). That the SDMCC is underlain by continental crustal material is also supported by the presence of granitoids on Mt. Suckling (Davies and Smith, 1971), its proximity to the exposed Kagi Metamorphics of felsic composition to the southwest of Mt. Suckling (Fig. 3), and by its coincidence with a Bouguer gravity low (Geological Survey of Papua New Guinea and British Geological Survey, 2004; Milsom, 1973) that is continuous with the Kagi Metamorphics farther west.

1.4 Igneous rocks of the Suckling-Dayman metamorphic core complex

The SDMCC has been intruded by two plutonic suites. The older of these is the Yau Gabbro of Smith and Davies (1976); however, we refer to these rocks as the Yau Igneous Complex. They consist of metamorphosed tholeiitic gabbroic-tonalitic rocks that intrude the Goropu Metabasalt in the eastern part of the MCC (Fig. 3). The gabbroic-tonalitic rocks have previously been interpreted to comprise subvolcanic intrusions that are co-magmatic with the Late Cretaceous Goropu Metabasalt and Kutu Volcanics (Smith and Davies, 1976).

A younger plutonic suite consists of granitoids (*sensu lato*) that have calc-alkaline to shoshonitic compositions (Suckling Granite, Mai'iu Monzonite, Bonua Porphyry; Smith and Davies, 1976). These stock-like bodies intrude the western part of the core complex near Mt. Suckling (Fig. 3). Geochemically, the Suckling Granite may be distinguished from Mai'iu Monzonite and Bonua Porphyry (see section 3.2). Stream boulders derived from erosion of these granitoids have been dated, yielding apparent ages of 10.8 ± 0.8 and 9.4 ± 0.8 Ma for hornblende, and 3.3 ± 0.1 Ma for biotite from two samples of Suckling Granite (1*, Fig. 3) using the K–Ar method (Davies and Smith, 1974). More recently, Daczko et al. (2011) reported a single zircon U–Pb LA-ICP-MS age of 3.3 ± 0.1 Ma from a granite boulder collected in the Mai'iu River near the range front (in the hanging wall) due north of Mt. Dayman (2*, Fig. 3). The Mai'iu Monzonite comprises coarse-grained granodiorite, adamellite, monzonite and hornblendite (Smith and Davies, 1976). Hornblende from two Mai'iu Monzonite stream boulders (3*, Fig. 3) yielded apparent K–Ar ages of 6.3 ± 0.4 and 4.4 ± 0.4 Ma, respectively (Davies and Smith, 1974). Lastly, small stocks of the

Bonua Porphyry to the south of the SDMCC consist of hornblende, biotite and/or pyroxene-bearing porphyritic microdiorite and micromonzonite where they intrude mafic and ultramafic rocks of the Goropu Metabasalt and PUB, respectively (Smith and Davies, 1976). K–Ar dating of biotite from a single stream boulder of Bonua Porphyry (4*, Fig. 3) yielded an apparent age of 5.3 ± 0.2 Ma (Davies and Smith, 1974).

Rare undeformed mafic dikes and sills of probable Quaternary age are locally present in the footwall adjacent to the trace of the Mai'iu Fault (Fig. 3; Little et al., 2019; this study). Daczko et al. (2011) inferred that the dikes intruded the mylonites shortly after cessation of ductile movement but under a similar stress regime that created the extensional fabric of the latter. Little et al. (2019), on the other hand, noted their chilled margins and lack of deformation, and inferred a post-mylonitic intrusive age, suggesting that they are feeder dikes similar to those supplying the Holocene basaltic andesite eruptions at Goropu Crater along the Mai'iu Fault (Fig. 3). The youngest phase of igneous activity includes the pyroclastic absarokites and shoshonites of the Sesagara Volcanics in the hanging wall of the Mai'iu Fault, which are possibly as young as Holocene (Smith and Davies, 1976), and the pyroclastic shoshonites of the Waiowa Volcanics that erupted from Goropu Crater in 1943 and 1944 (Baker, 1946; Fig. 3). Hydrothermal springs occur along the Mai'iu Fault (Fig. 3) and are presumably driven by heating of groundwater due to rapid exhumation of still-hot footwall rocks at depth (Latter, 1964; Little et al., 2019).

2. Methods

2.1 Whole rock major oxide and trace element analysis

Rocks were powdered in an agate mill. Elemental concentrations were determined on fused glass disks using a 10:1 flux (lithium borate) to sample ratio with a 1 KW Bruker S8 Tiger wavelength dispersive X-ray fluorescence (WDS-XRF) analyzer at the University of Waikato, New Zealand. For trace element analysis, representative samples were dissolved in NH_4F for 60 hours at 210°C (Hu et al., 2013). Trace element concentrations were measured on a Thermo Scientific Element2 HR-ICP-MS housed at Victoria University Wellington, New Zealand. An in-house gravimetric multi-element synthetic mixture was employed to calibrate the unknowns and to monitor machine drift. A secondary reference material (AGV-2) served to determine the accuracy of the unknowns. Accuracies are typically <10% for most elements and the measured AGV-2 values typically overlap with those recommended by USGS at the 2s level. Accuracies of elements that did not overlap with the recommended values at 2s level are Ba (~9%), Er (~18%), Ga (~12%), Gd (~18%), La (~7%), Sr (~8%), Tb (~15%) and Zr (~11%). Trace elements were considered below the detection limit if their concentrations were within error of three times the standard deviation of the procedural blank.

2.2 LA-ICP-MS zircon U–Pb depth-profile analysis

Zircons were depth-profiled (time-resolved) in order to monitor multiple U–Pb age domains (e.g., inherited cores and late-stage rims) following procedures

described in Marsh and Stockli (2015) and because of the convenience for subsequent double-dating of the zircons with (U-Th[-Sm])/He (results not reported here). Zircon grains were sprinkled or picked onto double-sided adhesive tape on 1" acrylic disks for LA-ICP-MS U–Pb analyses performed at the UTChron Laboratories of the University of Texas at Austin. Approximately 50 zircon grains (where available) from each sample were ablated with a 30-µm spot size using a Photon Machines Analyte G2 193 nm excimer laser coupled to a Thermo Scientific Element2 HR-ICP-MS. Each analysis included 4 pre-ablation surface cleaning shots, 25 sec baseline data collection, 30 sec laser dwell time and 35 sec washout. Energy and repetition rate were 4 mJ and 10 Hz, respectively. GJ-1 zircon ($^{206}Pb/^{238}U$ age = 601.7 ± 1.3 Ma; Jackson *et al.*, 2004) served as the internal zircon standard and was interspersed with unknown zircons at a 1:5 ratio. Plešovice ($^{206}Pb/^{238}U$ age = 337.13 ± 0.37 Ma; Sláma *et al.*, 2008), and Pak1 ($^{206}Pb/^{238}U$ age = 43.03 ± 0.01 Ma; in-house) were used as secondary reference material. Approximately 25 grains of feldspar were analyzed by LA-ICP-MS on polished thin sections of two samples of the Suckling Granite and one of the Mai'iu Monzonite. Analytical conditions were identical those from the zircon U–Pb analyses, but analyses were shortened (10 sec laser dwell time) to avoid drilling through the feldspars. Reduction of the isotopic raw data was performed in Iolite software with the IgorPro package (Paton et al., 2011) and VizualAge data reduction scheme (Petrus and Kamber, 2012) that allows the data to be corrected for instrumental drift and down hole fractionation. Data visualization and age calculations were performed in IsoplotR (Vermeesch, 2018) using decay constants as recommended by the IUGS Subcommission in Geochronology (Steiger and Jaeger, 1977) and adapting a $^{238}U/^{235}U$ value of 137.824 for GJ-1 (Hiess et al., 2012). Due to isobaric interferences in the

measurement of ^{204}Pb, a ^{204}Pb-based correction could not be applied. However, due to careful inspection of isotopic signals in Iolite software it was possible to identify cosmic spikes and zones of high common Pb (Pb_c) and avoid them by shortening the integration window accordingly. $^{206}Pb/^{238}U$ analyses were corrected for the effects of initial ^{230}Th disequilibrium (Schärer, 1984) based on whole-rock Th/U (1.9-4.4 where available, two asterisks in Table 3) or assuming $Th/U_{magma} = 3$ (single asterisk in Table 3). Propagation of systematic and random errors was performed in accord with a workflow proposed by Horstwood et al. (2016). All single-grain dates are reported at the 2SE (standard error) confidence level. They are generally reported as $^{206}Pb/^{238}U$ dates, but if they are >1 Ga, the corresponding $^{207}Pb/^{206}Pb$ date is given in addition. No discordance filter was applied. Ages of the individual samples were calculated from the lower intercepts in Tera-Wasserburg concordia plots by anchoring the upper intercepts at $^{207}Pb/^{206}Pb = 0.83$. This value is based on $^{207}Pb/^{206}Pb$ analyses of co-genetic feldspars (Table S2) from samples of the Suckling Granite (0.8324 ± 0.00808, PNG-15-61a; 0.8361 ± 0.01025, PNG-15-64a) and Mai'iu Monzonite (0.8350 ± 0.01196, PNG-15-66a) and is consistent with the values ($^{207}Pb/^{206}Pb$ ~ 0.8421-0.8357) predicted from the two-stage Pb evolution model of Stacey and Kramers (1975) for rocks with ages <100 Ma. The Tera-Wasserburg lower-intercept ages are reported at the 95% confidence level excluding and including systematic errors (separated by a slash in the text, e.g., ± 1/2 Ma; Table 3). Final age calculations were performed on groups of U–Pb analyses that appear to define a single (sub-)population in Tera-Wasserburg (including those that overlap with the discordia line), kernel density estimation (KDE) and cumulative age distribution (CAD) plots. Discordancy of a U–Pb analysis (expressed in %) is reported as the ratio of its $^{206}Pb/^{238}U$ date divided by its $^{207}Pb/^{235}U$ date (Table S1).

3. Results

3.1 Outcrop relationships and petrography

Outcrops of the units described below (Yau Igneous Complex, Suckling Granite, Mai'iu Monzonite, Bonua Porphyry, basaltic andesite dikes) are of variable quality. Exposure is most widespread proximal to the modern fault scarp where undeformed basaltic andesite dikes intrude the Goropu Metabasalt in the footwall of the SDMCC (Table 1, Figs. S3a and b). Farther south and up-dip of the Mai'iu Fault trace, vegetation covers most of the footwall. Our samples of the Yau Igneous Complex, Suckling Granite, Mai'iu Monzonite, Bonua Porphyry, and igneous clasts in the Gwoira Conglomerate were collected in river cuts or, locally, on ridge outcrops (Figs. S3c-n). Due to the sparse exposure of the units referred to above, little can be said about the internal structure of the plutonic complexes.

Smith and Davies (1976) refer to metamorphosed gabbroic, doleritic and tonalitic rocks (Table 1) that crop out between Mts. Dayman and Masasoru (Fig. 3) as the Yau Gabbro. Based on the occurrence of both gabbroic and tonalitic rocks in this suite, we suggest the name be revised to Yau Igneous Complex. We also include a plagioclase-rich cumulate of tholeiitic composition (PNG-16-41a, Tables 1 and 2) into the Yau Igneous Complex. Cataclastic deformation and dynamic recrystallization of quartz affect doleritic samples in the Yau Igneous Complex (Fig. 4a), whereas coarser-grained gabbroic (Fig. 4b) and tonalitic (Fig. 4c) rocks appear

less deformed. This difference in deformation intensity correlates with the vertical proximity of the samples to the exhumed Mai'iu Fault surface as expressed by the smooth and planar topography of Mt. Dayman; that is, the deformed dolerites come from a structural level closer to the abandoned fault plane than the coarse-grained undeformed gabbros and tonalites.

Table 1: Petrography of the igneous rocks of the Suckling-Dayman metamorphic core complex.

Map unit	Sample ID	Sample type	Longitude [E]†	Latitude [S]†	Elevation [m]	Rock type	Mineral assemblage
Suckling Granite	PNG-15-61a	outcrop	149° 1' 39.1"	9° 41' 45.6"	3410	Granodiorite[1]	pl (ab) + qtz + wmca + Fe-oxides + ttn + ap + zrn
	PNG-15-64a	outcrop	148° 58' 51.3"	9° 43' 12.1"	3450	Qtz-monzodiorite[1]	pl + qtz + kfs + bt + Fe-oxides + py + ttn + ap + zrn + aln-(Ce)
	AU51087*	float	149° 0' 5"	9° 44' 10.2"	2470	Qtz-monzodiorite[1]	pl + qtz + kfs + bt + am + Fe-Ti-oxides + ttn + ap + zrn
	AU51088*	float	149° 0' 5"	9° 44' 10.2"	2470	Qtz-monzodiorite[2]	pl + qtz + kfs + bt + am + Fe-Ti-oxides + ttn + ap + zrn
	AU51089*	float	149° 0' 5"	9° 44' 10.2"	2470	Qtz-monzodiorite[2]	pl + qtz + kfs + bt + am + Fe-Ti-oxides + ttn + ap + zrn
Mai'iu Monzonite	PNG-15-66a	outcrop	149° 1' 14.3"	9° 45' 58.2"	2045	Qtz-monzodiorite[1]	pl + qtz + kfs + bt + am + cpx + Fe-Ti oxides + ttn + ap + zrn
	PNG-16-2a	outcrop	149° 3' 43.1"	9° 44' 28.7"	1675	Qtz-monzodiorite[1]	pl + qtz + kfs + bt + am + Fe-Ti oxides + ttn + ap + zrn + Fe-sulfides
	PNG-16-159b	outcrop	148° 59' 23.9"	9° 42' 56.1"	3380	Monzodiorite[1]	pl + qtz + kfs + bt + am + Fe-Ti oxides + ttn + ap + zrn
	PNG-16-163a	outcrop	149° 3' 10.7"	9° 45' 58.8"	1835	Hornblendite[2]	pl + kfs + bt + am + Fe-Ti oxides + ttn + ap + zrn
	PNG-16-174a	float	149° 15' 3.7"	9° 42' 9.7"	1070	Monzonite[1]	pl (ab) + qtz + kfs + am + chl + Fe-Ti oxides
Bonua Porphyry	PNG-16-157a	outcrop	149° 5' 17.4"	9° 54' 45.8"	270	Monzonite[1]	kfs + bt + cpx (di) + cal + chl + Fe-Ti oxides + ttn + ap + zrn + py
	AU51095*	outcrop	149° 9'38"	9° 55' 39.4"	220	Latite[1]	bt + cpx + opx + srp + opaques
Yau Igneous Complex	PNG-15-3b	outcrop	149° 18' 34.1"	9° 49' 45.1"	2290	Gabbro/Dolerite[1]	pl + cpx (di-aug) + pmp + chl + ep + qtz + py + Fe-Cu sulfides
	PNG-15-4a	outcrop	149° 18' 8.1"	9° 51' 28.2"	2500	Gabbro/Dolerite[1]	pl + cpx (di-aug) + pmp + chl + ep + qtz + ttn + py + Fe-Ti oxides + Cu-sulfides
	PNG-15-41b T2	float	149° 24' 37.9"	9° 41' 49.4"	140	Qtz-gabbro[2]	pl + am + qtz + pmp + prh(?) + chl + ttn + Fe-Ti oxides + zrn + ap
	PNG-15-54b T2	clast	149° 29' 0.2"	9° 46' 59.5"	220	Qtz-gabbro[2]	pl + relic px + am + qtz + pmp + prh(?) + chl + Fe-Ti oxides + ap + ttn + zrn + py
	PNG-15-54c T2	clast	149° 29' 0.2"	9° 46' 59.5"	220	Qtz-gabbro[2]	pl + am + qtz + pmp + prh(?) + chl + Fe-Ti oxides + ap + ttn + Cu-Fe-sulfides + bdy
	PNG-16-41a	clast	149° 28' 11.0"	9° 49' 34.3"	410	Pl-px cumulate[2]	pl + cpx (di-aug) + qtz + chl + pmp + py + ap + ttn + zrn + Fe-Ti oxides + Fe-Cu-sulfides
	PNG-16-108b	clast	149° 27' 58.1"	9° 46' 22.8"	155	Qtz-gabbro[1]	pl + am + cpx (Fe-aug, Fe-pgt) + qtz + cal + prh + chl + Fe-Ti oxides + ap
	PNG-16-128a	clast	149° 26' 54.6"	9° 45' 41.5"	275	Qtz-gabbro[2]	pl + px + am + qtz + chl + ap + opaques
	PNG-16-156a	clast	149° 33' 48.9"	9° 50' 29.0"	200	Qtz-gabbro[1]	pl + cpx (Fe-aug, aug) + chl + ap + Fe-Ti oxides + ttn
	PNG-16-1008a	outcrop	149° 26' 2.1"	9° 56' 5.3"	1160	Tonalite[1]	pl + am + qtz + Fe-Ti oxides + ap + zrn
	PNG-16-1029a	clast	149° 29' 1.6"	9° 52' 8.6"	440	Tonalite[1]	pl + am + cpx (Fe-aug, Fe-pgt) + qtz + chl + pmp + prh + Fe-Ti oxides + ap
	AU51082*	float	149° 19' 59"	10° 2' 12.1"	190	Tonalite[1]	pl + am + qtz + px + prh + pmp + opaques + ap
Dikes	PNG-15-60a	outcrop	149° 16' 7.1"	9° 40' 38.9"	230	Basaltic andesite[1]	pl (ab) + cpx (di) + bt + ttn + chl + pmp + py
	PNG-16-150c	outcrop	149° 17' 38.8"	9° 40' 52.1"	270	Basaltic andesite[1]	pl + am + relic px + qtz + chl + kfs + ttn + cal + py

†: Reference datum AGD1966, AMG Zone 55.
Sample type: 'clast' refers to gabbroic-tonalitic rock clast in the Gwoira Conglomerate; 'float' refers to stream or landslip boulder.
*: Sample location approximated from aerial photographs.
[1]: Rock type based on bulk composition (Fig. S5).
[2]: Rock type based on petrography.
Abbreviations after Siivola and Schmid (2007): ab – albite, act – actinolite, aln-(Ce) – allanite-(Ce), am – amphibole, ap – apatite, aug – augite, bt – biotite, cal – calcite, chl – chlorite, cpx – clinopyroxene, di – diopside, ep – epidote, kfs – K-feldspar, opx – orthopyroxene, pgt – pigeonite, pl – plagioclase, pmp – pumpellyite, prh – prehnite, px – pyroxene, py – pyrite, qtz – quartz, srp – serpentine, ttn – titanite, wmca – white mica, zrn – zircon; bdy – baddeleyite (Whitney and Evans, 2010).
Note, the order of minerals in column "Mineral assemblage" does not reflect relative abundances.

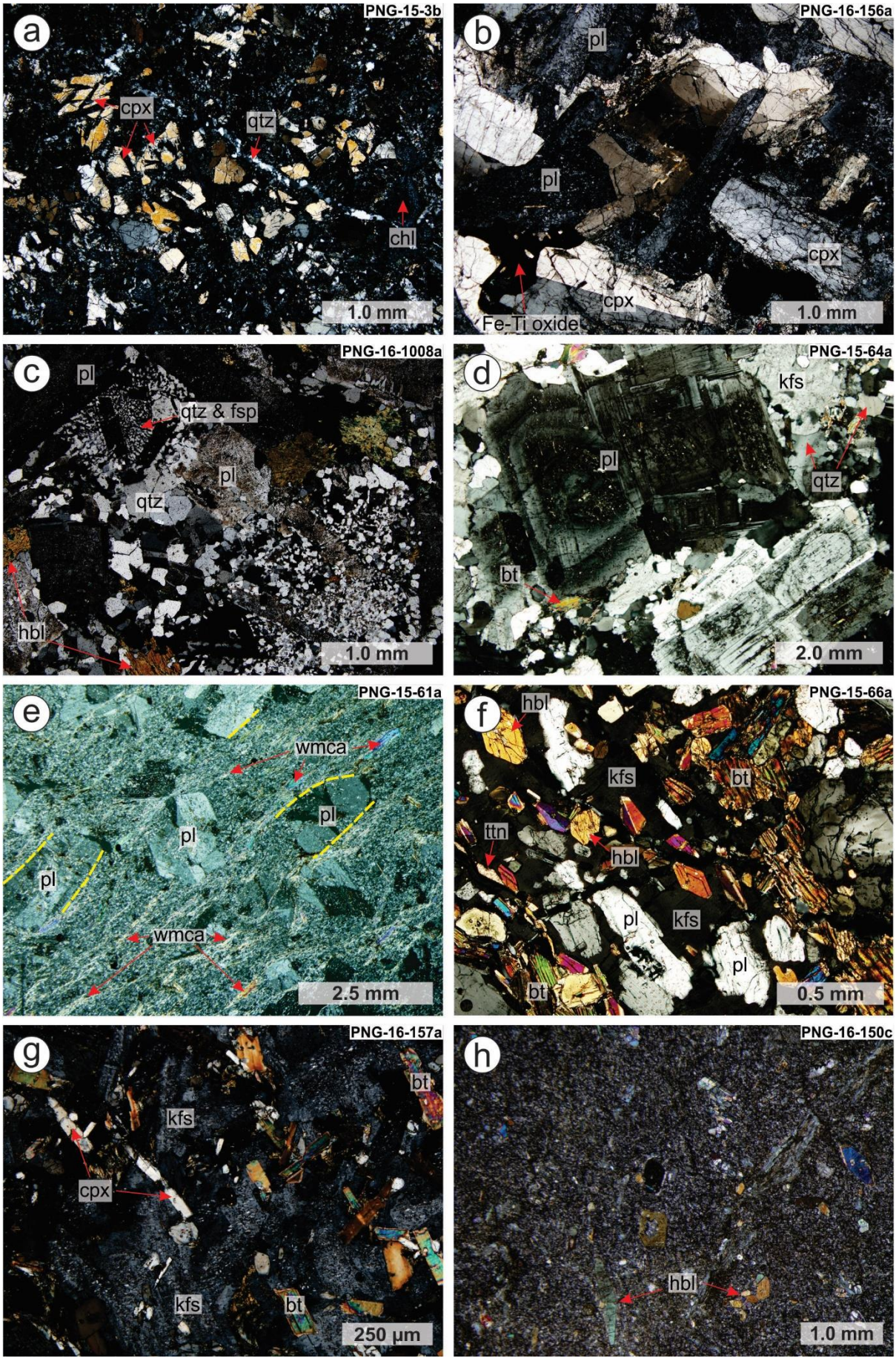
a
PNG-15-3b
cpx
qtz
chl
1.0 mm
b
PNG-16-156a
pl
pl
cpx
cpx
Fe-Ti oxide
1.0 mm
c
PNG-16-1008a
pl
qtz & fsp
pl
qtz
hbl
1.0 mm
d
PNG-15-64a
kfs
pl
qtz
bt
2.0 mm
e
PNG-15-61a
wmca
pl
pl
pl
wmca
2.5 mm
f
PNG-15-66a
hbl
kfs
bt
ttn
hbl
pl
kfs
pl
bt
0.5 mm
g
PNG-16-157a
bt
kfs
cpx
kfs
bt
250 µm
h
PNG-16-150c
hbl
1.0 mm

Fig. 4: Photomicrographs of igneous rock units from the Suckling-Dayman metamorphic core complex. (a) Dolerite consisting of clinopyroxene in a fine-grained matrix of plagioclase showing cataclastic deformation (e.g., disrupted clinopyroxenes) and a dynamically recrystallized quartz vein. (b) Quartz-gabbro consisting principally of clinopyroxene (locally twinned), altered plagioclase (albite and relics of anorthite) and Fe-Ti oxides. (c) Tonalite with granophyric-like texture (consisting of quartz and feldspar) and altered, cloudy plagioclase and hornblende. (d) Relatively undeformed Suckling Granite with phenocryst of plagioclase (zoned), K-feldspar, quartz and biotite. (e) Deformed Suckling Granite showing plagioclase (albite-rich) phenocrysts in a fine-grained groundmass of quartz, plagioclase and foliae of white mica. (f) Mai'iu Monzonite showing poikilitic textures with chadacrysts of hornblende, titanite, plagioclase and biotite enclosed in oikocrysts of K-feldspar. (g) Bonua Porphyry consisting principally of clinopyroxene, biotite and (felty) K-feldspar. (h) Amphibole-phyric basaltic andesite dike with a fine-grained quartzofeldspathic groundmass. Mineral abbreviations after Siivola and Schmid (2007).

Samples collected from the Suckling Granite (Fig. 4d), Mai'iu Monzonite (Fig. 4f), Bonua Porphyry (Fig. 4g), as well as rare basaltic andesite dikes (Fig. 4h) exposed in the mylonitic parts of the footwall, are mostly undeformed. They generally have normal igneous textures, but samples of the Mai'iu Monzonite include cumulate-like rocks (e.g., hornblendite, PNG-16-163a; Table 1). The microstructure of a deformed sample from the Suckling Granite (Fig. 4e) indicates a progression from magmatic to ductile solid-state deformation as suggested by a shape-preferred

orientation of feldspar phenocrysts surrounded by a foliated groundmass containing recrystallized seams of white mica (Figs. 4e and S4). All samples of the Suckling Granite, Mai'iu Monzonite, Bonua Porphyry and the basaltic andesite dikes show low-grade alteration, as evidenced, for example, by the replacement of biotite by chlorite. Petrographically, the Suckling Granite includes sub-units with variable abundances of mafic minerals. Some contain biotite and hornblende, while others have only biotite, and still others neither biotite nor hornblende, but white mica (Table 1). Compared to the Suckling Granite, the Mai'iu Monzonite contains less quartz and K-feldspar but more mafic phases (biotite, hornblende, rare clinopyroxene) and accessory minerals (e.g., zircon, apatite). The Bonua Porphyry contains clinopyroxene and biotite as dominant mafic phases and K-feldspar instead of plagioclase as the prevailing feldspar. Decimeter-thick basaltic andesite dikes intruding the footwall near the Mai'iu Fault trace contain porphyritic hornblende and clinopyroxene, and have chilled margins against the mylonitically deformed Goropu Metabasalt. For more detailed petrographic descriptions of these rock units, the reader is referred to the supplementary material.

3.2 Whole-rock geochemistry

Rock classification

Major oxide and trace element compositions of igneous rocks from the several suites are presented in Table 2. The analyses yielded loss on ignition (LOI) values ranging from 0.44 to 4.91 wt%, consistent with the rocks having experienced low-

grade metamorphism. In a diagram of Co vs. Th (Hastie et al., 2007)—topologically similar to the K_2O vs. SiO_2 diagram of Peccerillo and Taylor (1976), but less susceptible to alteration—samples of the Goropu Metabasalt and the Yau Igneous Complex plot in the basalt, basaltic andesite/andesite and dacite/rhyolite fields (corresponding to gabbro, gabbro/diorite and granodiorite/granite in plutonic terminology), straddling the boundary between the tholeiitic and calc-alkaline series (Fig. 5a). One quartz-gabbro (PNG-16-108b) and two tonalite (AU51082, PNG-16-1008a) samples of the Yau Igneous Complex that plot exclusively in the dacite/rhyolite field of the calc-alkaline series (blue hexagons in Fig. 5a), correspond to higher SiO_2 concentrations (55.52-63.23 wt%, Table 2) and are, in the following, referred to as the 'high-silica suite'. Two dolerites (PNG-15-3b, PNG-15-4a), one quartz-gabbro (PNG-16-156a) and a tonalite (PNG-16-1029a) that lie in the basaltic field and straddle the boundary between the tholeiitic and calc-alkaline series (purple hexagons in Fig. 5a) are referred to as the 'low-silica suite'. Samples of the Suckling Granite lie in the dacite/rhyolite field just below the boundary between the calc-alkaline and high-K calc-alkaline to shoshonite series (Fig. 5a). The Mai'iu Monzonite, Bonua Porphyry and basaltic andesite dikes predominantly plot in the high-K calc-alkaline to shoshonite series with overall basaltic compositions (Fig. 5a).

A similar relative geochemical attribution of the units is evident from a total alkali silica diagram (Fig. 5b; Le Maitre et al., 2002). Samples of the Goropu Metabasalt, Yau Igneous Complex, Suckling Granite and the basaltic andesite dikes plot in the subalkaline magmatic series, whereas those from the Mai'iu Monzonite and the Bonua Porphyry mostly occupy fields in the alkaline magmatic series (Fig. 5b). Most of the samples have a metaluminous composition (Fig. S6) using the

classification of Shand (1947). Two samples of the Suckling Granite (PNG-15-61a, PNG-15-64a) are peraluminous. They have aluminium saturation indices (ASI) > 1.1 (Fig. S6), classifying them as S-type granitoids (Chappell and White, 1974).

Table 2: Whole-rock compositional data of the igneous rocks of the Suckling-Dayman metamorphic core complex.

Sample	Yau Igneous Complex								Suckling Granite		
	AU 51082	PNG-15-3b	PNG-15-4a	PNG-16-41a	PNG-16-108b	PNG-16-156a	PNG-16-1008a	PNG-16-1029a	AU 51087	PNG-15-61a	PNG-15-64a
wt%											
SiO_2	56.34	46.65	46.92	45.08	55.52	49.23	63.23	53.41	68.70	68.92	66.91
Al_2O_3	12.90	14.13	13.71	19.73	12.90	12.31	13.09	13.77	15.73	16.74	17.63
TiO_2	1.54	1.60	1.48	1.58	1.54	2.60	0.77	1.27	0.32	0.38	0.32
MnO	0.25	0.18	0.21	0.13	0.23	0.25	0.15	0.19	0.04	0.03	0.03
FeO_t	14.67	12.08	13.50	10.99	14.38	14.04	10.96	14.10	2.22	2.74	2.14
MgO	1.47	7.83	6.74	4.84	1.62	4.02	0.91	3.30	1.12	0.84	0.98
CaO	5.72	9.92	9.92	12.38	5.87	9.56	4.29	7.70	2.22	0.45	1.61
Na_2O	3.73	2.71	3.17	2.24	4.79	3.23	4.51	2.87	5.15	4.37	5.34
K_2O	0.62	0.30	0.08	0.06	0.33	0.08	0.20	0.10	3.50	2.93	3.36
P_2O_5	0.52	0.17	0.15	0.05	0.63	0.23	0.27	0.13	0.15	0.18	0.17
SO_3	0.04	0.32	0.06	0.31	0.02	0.01	0.03	0.11	0.02	0.01	0.02
SrO	0.01	0.01	0.02	0.01	0.01	0.01	0.01	0.01	0.16	0.03	0.21
BaO	0.02	0.01	0.02	0.01	0.01	0.02	0.01	0.01	0.09	0.09	0.10
LOI	1.57	3.35	3.24	1.29	1.67	3.62	1.54	2.33	0.44	2.79	2.10
Total	99.39	99.28	99.21	98.71	99.53	99.21	99.95	99.30	99.90	100.50	100.96
ppm											
Li	4.78	10.73	12.84	1.66	2.65	3.08	2.81	5.73	11.41	7.62	7.14
Rb	14.2	4.9	2.7	0.7	4.1	1.5	1.9	1.4	71.0	76.0	67.6
Sr	206	189	231	180	140	138	128	119	1561	335	1750
Y	115.30	25.70	27.45	7.23	92.16	55.32	99.23	28.50	7.33	7.09	4.97
Zr(90)*	453.51	97.12	88.45	11.79	368.60	182.25	422.22	67.72	45.97	163.87	118.19
Nb	22.86	6.28	5.00	0.66	18.03	10.67	21.55	1.73	6.90	9.21	7.58
Cs	0.12	0.19	0.27	0.12	0.03	0.04	0.14	0.13	2.08	2.10	1.83
Ba	104	32	104	10	55	23	58	23	941	857	931
La	26.83	5.56	5.25	0.82	19.75	7.30	22.50	3.30	23.12	20.71	19.70
Ce	69.07	14.18	13.04	2.12	51.07	20.78	58.21	8.79	44.62	36.08	37.24
Pr	10.04	2.11	1.98	0.34	7.54	3.35	8.33	1.38	4.92	4.35	4.17
Nd	50.17	10.87	10.46	1.98	38.78	18.41	41.64	7.56	18.05	16.21	15.74
Sm	14.97	3.47	3.39	0.76	11.83	6.15	12.25	2.65	3.11	2.88	2.78
Eu(151)*	4.39	1.27	1.28	0.57	3.64	2.29	3.35	0.99	1.02	0.96	1.01
Gd	17.68	4.13	4.21	1.01	14.14	7.70	14.35	3.55	2.86	2.73	2.43
Tb	3.30	0.79	0.82	0.21	2.66	1.52	2.74	0.73	0.33	0.34	0.28
Dy	21.53	5.10	5.26	1.45	17.31	10.08	17.79	5.15	1.53	1.52	1.19
Ho	4.61	1.09	1.13	0.31	3.67	2.19	3.84	1.15	0.28	0.27	0.20
Er	13.88	3.12	3.33	0.91	10.97	6.53	11.71	3.54	0.85	0.79	0.61
Tm	1.99	0.45	0.48	0.13	1.58	0.96	1.73	0.53	0.11	0.10	0.08
Yb	12.70	2.76	2.99	0.82	10.10	6.10	10.87	3.52	0.68	0.64	0.50
Lu	1.98	0.42	0.47	0.13	1.57	0.96	1.69	0.55	0.10	0.10	0.08
Hf	12.32	2.56	2.57	0.40	9.29	4.76	10.68	1.94	1.62	5.11	3.45
Ta	2.28	0.53	0.68	0.15	1.50	0.91	1.73	0.17	0.88	0.73	0.57
Pb	0.31	0.43	0.20	0.07	0.18	0.17	0.64	0.23	48.26	34.89	142.97
Th	2.36	0.29	0.34	bdl	1.74	0.67	2.14	0.22	5.88	8.27	7.70
U	0.66	0.13	0.11	0.01	0.52	0.23	0.64	0.11	1.55	4.35	3.49
Sc	29.01	44.07	51.98	34.27	25.95	50.26	15.13	37.98	4.02	3.34	3.31
V	12	324	412	741	12	817	2	543	41	43	39
Cr	2	301	191	1	1	2	5	9	167	59	64
Co	20.43	45.96	55.24	45.07	16.78	45.95	8.84	42.21	6.18	5.43	3.96
Ni	bdl	67	79	37	bdl	28	bdl	16	742	49	9
Cu	1.71	102.71	196.07	63.89	1.43	5.68	1.62	81.50	2.90	6.19	19.01
Zn	128.77	95.59	82.71	64.28	208.69	81.46	74.26	117.12	40.39	57.92	38.25
Ga	33.32	17.82	19.95	21.84	26.50	23.54	24.81	20.71	22.90	24.83	22.41

	Mai'iu Monzonite (plutonic)				dike	Bonua Porphyry		Bas. andesite dikes		Goropu Metabasalt	
Sample	PNG-15-66a	PNG-16-159b	PNG-16-163a	PNG-16-174a	PNG-16-2a	PNG-16-157a	AU 51095	PNG-15-60a	PNG-16-150c	PNG-16-17z	PNG-16-17.2d
wt%											
SiO_2	55.10	49.88	48.51	51.29	61.14	51.58	46.19	54.19	56.07	48.84	45.56
Al_2O_3	14.07	16.24	14.17	15.84	16.68	14.09	12.60	12.40	14.73	12.32	14.74
TiO_2	1.26	1.38	1.74	1.32	0.84	1.51	1.59	1.06	0.99	1.63	1.33
MnO	0.11	0.13	0.13	0.11	0.07	0.12	0.12	0.11	0.12	0.22	0.19
FeO_t	7.07	8.99	9.18	7.41	4.82	7.53	8.26	6.65	6.72	11.95	11.45
MgO	7.55	5.72	7.80	6.77	4.01	5.84	8.97	10.06	7.18	6.75	7.60
CaO	6.49	6.14	7.19	5.22	4.44	5.47	7.67	6.00	4.16	9.37	11.49
Na_2O	3.55	3.55	3.22	3.96	4.37	3.50	2.01	4.35	3.52	2.96	2.08
K_2O	2.19	3.24	2.16	3.47	2.90	4.92	5.05	0.34	2.64	0.04	0.14
P_2O_5	0.60	0.87	0.92	0.64	0.26	0.65	1.04	0.52	0.33	0.19	0.14
SO_3	0.02	0.03	0.02	0.03	0.03	1.45	0.34	0.26	0.07	0.17	0.07
SrO	0.14	0.23	0.17	0.09	0.13	0.10	0.16	0.05	0.02	271.00	82.00
BaO	0.07	0.10	0.09	0.09	0.08	0.14	0.18	0.01	0.04	81.00	94.00
LOI	2.60	2.72	3.92	3.18	1.32	3.52	4.70	3.87	3.20	4.91	4.24
Total	100.84	99.28	99.26	99.44	101.13	100.45	98.93	99.87	99.78	99.38	99.04
ppm											
Li	10.88	11.97	10.33	9.25	15.40	6.72	12.41	26.21	17.91	nd	11.39
Rb	64.7	94.0	70.3	75.1	65.0	173.1	120.4	7.2	68.4	0.3	2.9
Sr	1262	2189	1645	970	1156	952	1443	493	195	280	141
Y	17.14	16.25	22.93	20.68	9.47	16.24	19.00	20.54	17.96	23.65	22.08
Zr(90)*	53.08	117.93	65.44	383.34	169.58	298.41	424.86	464.81	266.18	104.55	80.88
Nb	11.68	9.80	13.74	15.22	5.77	18.26	17.10	8.12	8.50	6.65	4.80
Cs	2.62	3.61	2.58	0.17	1.75	2.42	6.08	0.29	1.30	0.03	0.05
Ba	656	955	855	848	759	1224	1535	114	373	22	17
La	42.03	34.23	52.26	54.29	19.15	59.23	59.20	58.87	29.92	6.19	4.67
Ce	90.01	71.89	115.73	108.37	38.75	125.10	125.51	130.68	62.74	15.77	11.89
Pr	11.00	8.76	14.04	12.60	4.40	14.02	14.53	15.69	7.41	2.34	1.79
Nd	45.12	36.10	56.86	49.25	17.44	52.93	57.17	64.20	29.88	11.42	9.34
Sm	8.00	6.88	10.02	8.27	3.33	8.05	9.55	12.09	5.83	3.36	3.04
Eu(151)*	2.27	2.17	2.81	2.37	1.18	2.39	2.76	3.01	1.61	1.26	1.15
Gd	7.33	6.46	9.50	8.07	3.28	8.01	8.68	10.32	5.57	4.03	3.66
Tb	0.88	0.80	1.17	0.96	0.42	0.90	1.02	1.19	0.76	0.79	0.68
Dy	3.98	3.72	5.37	4.45	2.07	3.83	4.38	4.87	3.88	4.89	4.41
Ho	0.71	0.67	0.95	0.80	0.39	0.67	0.77	0.81	0.73	1.02	0.91
Er	1.99	1.90	2.76	2.36	1.14	1.94	2.31	2.31	2.12	2.98	2.67
Tm	0.23	0.23	0.32	0.28	0.14	0.23	0.26	0.26	0.28	0.42	0.38
Yb	1.40	1.36	1.93	1.77	0.90	1.38	1.63	1.62	1.76	2.67	2.34
Lu	0.20	0.20	0.28	0.27	0.13	0.20	0.24	0.24	0.27	0.41	0.37
Hf	2.44	3.32	3.00	8.55	4.03	7.14	9.92	11.51	6.65	2.81	2.16
Ta	1.08	0.70	1.03	1.22	0.51	1.26	1.36	0.76	0.79	0.63	0.45
Pb	16.35	18.89	11.55	16.40	19.64	50.41	19.54	47.15	15.02	1.01	0.28
Th	14.32	3.91	5.25	11.39	7.66	8.16	10.65	20.44	8.93	0.56	0.21
U	3.23	1.22	1.33	2.83	2.48	2.65	2.85	4.67	2.60	0.18	0.10
Sc	20.71	23.59	29.17	21.38	12.00	18.62	22.83	18.51	19.07	33.89	41.95
V	162	216	237	190	106	214	207	161	142	290	309
Cr	375	134	371	395	129	273	484	843	479	201	309
Co	35.69	29.47	45.19	35.63	21.63	29.40	33.97	43.79	32.94	36.24	51.98
Ni	207	77	191	200	94	86	177	459	279	51	67
Cu	18.53	21.96	46.45	44.74	45.52	61.99	65.21	57.05	37.89	99.43	107.17
Zn	75.93	110.87	87.18	89.85	51.57	91.34	78.27	94.40	84.30	172.19	92.07
Ga	20.00	24.68	21.28	22.54	20.85	22.24	17.68	19.99	21.63	16.57	19.17

nd: not determined; bdl: below level of quantification; *: numbers in brackets denote the mass measured atomic mass.
Major elments in *wt%* determined by XRF. Trace elments in ppm determined by ICP-MS.

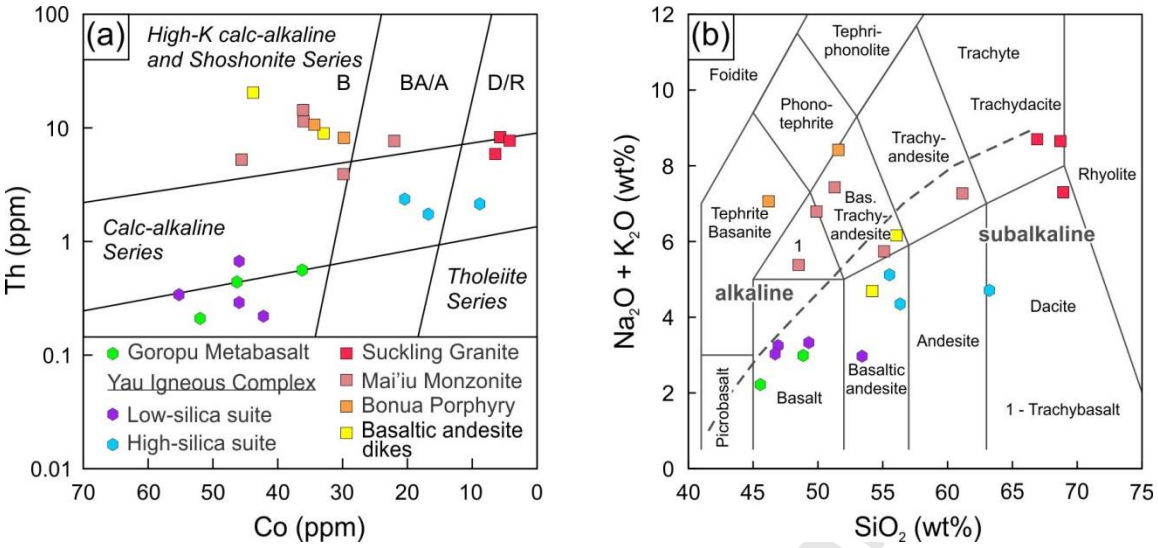

Fig. 5: Rock classification diagrams of the igneous rock units from the Suckling-Dayman metamorphic core complex after (a) Hastie et al. (2007) and (b) Le Maitre et al. (2002). Note, for convenience, extrusive and intrusive rocks have been plotted on the same diagrams. Abbreviations are: B – basalt, BA/A – basaltic andesite/andesite, D/R - dacite/rhyolite.

Whole-rock major oxide compositions (normalized to volatile-free compositions) of the various units reveal positive correlations of SiO_2 with Na_2O and Al_2O_3 and negative correlations with FeO_t, CaO, MgO, TiO_2 and P_2O_5 (Fig. S7). No systematic correlation of K_2O with SiO_2 is evident (Fig. S7b). The Suckling Granite, Mai'iu Monzonite, Bonua Porphyry, and one sample of the rangefront basaltic andesite dikes (PNG-16-150c) have high K_2O contents (2.16-5.05 wt%, Table 2) dissimilar to samples of the (predominantly tholeiitic-composition) Goropu Metabasalt and Yau Igneous Complex (0.04-0.62 wt%, Table 2). A second basaltic andesite dike (PNG-15-60a) has a lower K_2O content (0.34 wt%, Table 2); however, its field occurrence and trace element composition (see below) lead us to consider both of the basaltic andesite dikes to be part of the high-K suite. The unexpectedly

low K_2O content of PNG-15-60a can be explained by interaction of the rock with hydrothermal fluids leading to near-complete alteration of biotite (the main carrier of K_2O in this sample) to chlorite and removal of K from the system. Samples of the Goropu Metabasalt and the low-silica suite of the Yau Igneous Complex deviate from the trends defined by the Suckling Granite, Mai'iu Monzonite, Bonua Porphyry and the basaltic andesite dikes in SiO_2 vs. P_2O_5 and FeO_t (Figs. S7c and h). Too few samples of each unit are available to characterize fully their geochemical variability. However, rocks of the Yau Igneous Complex range in SiO_2 from ~45 to ~63 wt% (Table 2), indicating that the unit is internally differentiated. Similarly, rocks of the Mai'iu Monzonite have SiO_2 contents that vary from ~49 to ~61 wt% (Table 2)—again suggesting internal differentiation. In addition, local cumulate-like rocks such as the hornblendite PNG-16-163a contribute to the variability in SiO_2.

Trace element characteristics

The Yau Igneous Complex

Trace element data for the Yau Igneous Complex are depicted as chondrite-normalized rare earth element (REE; Fig. 6) and fertile mantle normalized multi-element (Fig. S8) diagrams. The dolerites of the low-silica suite (blue lines, Fig. 6) and the quartz-gabbro and tonalites of the high-silica suite (reddish lines, Fig. 6) have relatively flat chondrite-normalized REE patterns with slightly positive slopes ($[Ce/Yb]_{CN} > 1$). In particular the REE patterns of the dolerites closely resemble those from the Goropu Metabasalt (Fig. 6), yielding slightly enriched LEE patterns

($[Ce/Yb]_{CN} > 1$). On the other hand, the quartz-gabbro and tonalite samples of the low-silica suite (green lines, Fig. 6) show slightly negative slopes ($[Ce/Yb]_{CN} < 1$). All samples of the high-silica suite have higher abundances of the REE compared to the rocks of the low-silica suite and show negative Eu ($Eu/Eu^* = Eu_{CN} / [Sm_{CN} \times Gd_{CN}]^{0.5}$ = 0.8-0.9) anomalies (Fig. 6).

Rocks of the low-silica suite reveal elemental abundances that increase by about 2-4 orders of magnitude from highly compatible (HC) to very highly incompatible (VHI, Fig. S8a). Notable differences between the dolerites and the coarser-grained quartz-gabbro and tonalite samples of the low-silica suite include more pronounced positive V anomalies and negative Cr anomalies of the latter two (Fig. S8a). The trace element patterns of the low-silica suite differ from those of the high-silica suite (Fig. S8b). The latter reveal more step-like patterns with pronounced negative V and Ti anomalies and Cr and Ni values that are close to zero or below the detection limit (Fig. S8b, Table 2). Furthermore, samples of the high-silica suite exhibit prominent negative Sr ($Sr/Sr^* = Sr_{CN} / [Pr_{CN} \times Nd_{CN}]^{0.5}$ = 0.2-0.3, not shown) anomalies. The elemental patterns of the high-silica suite differ from those of the Goropu Metabasalt, whereas those from the low-silica suite—and in particular those of the dolerites—do resemble those of the Goropu Metabasalt well (Fig. S8).

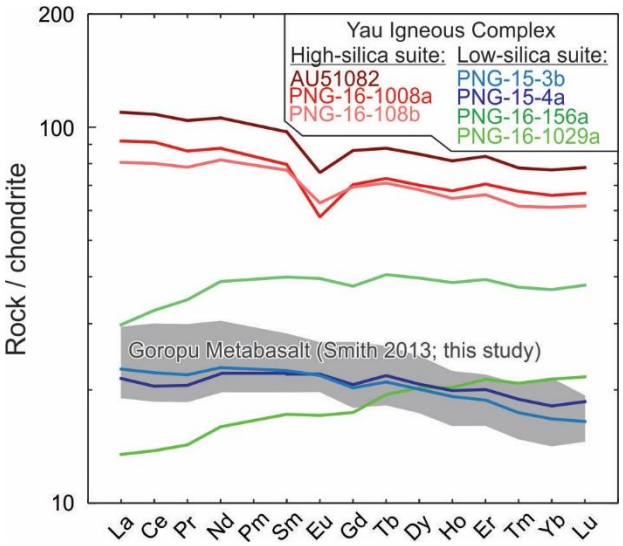

Fig. 6: Chondrite-normalized rare earth element (REE) diagram of the Yau Igneous Complex. Values of Pm were obtained from linear interpolation between Nd and Sm. Normalization values from Arevalo and McDonough (2010) and references therein. For reference, the range of REE values of the Goropu Metabasalt (data from this study and from Smith, 2013) is shown.

In a Nb/Yb vs. Th/Yb diagram after Pearce (2008), samples of the Yau Igneous Complex and the Goropu Metabasalt plot on the MORB-OIB array close to the composition of E-MORB (Fig. 7). Only one tonalite (PNG-16-1029a) of the low-silica suite plots above the MORB-OIB array close to the N-MORB composition (Fig. 7). For reference, published data from the Goropu Metabasalt, Kutu Volcanics and Emo Metamorphics on the Papuan Peninsula, and the Poya Terrane in New Caledonia are shown.

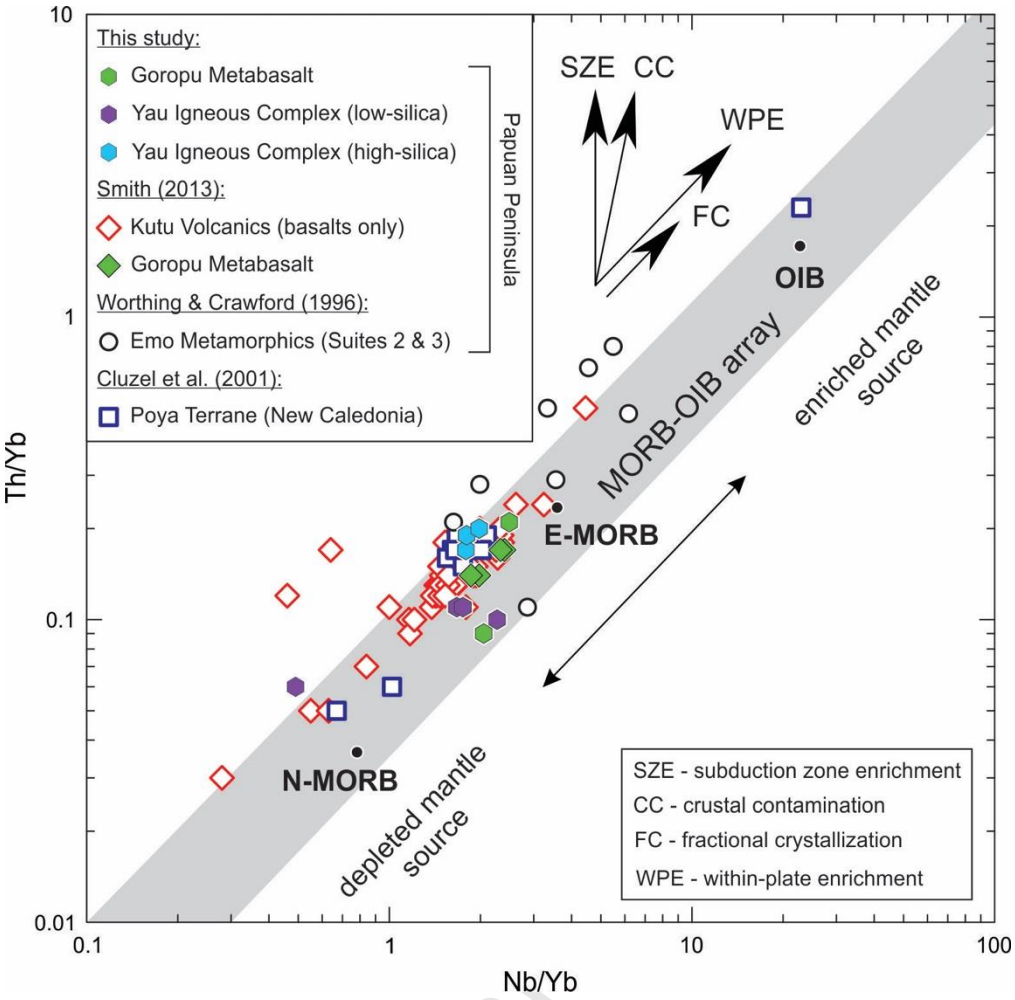

Fig. 7: Nb/Yb vs. Th/Yb diagram after Pearce (2008). For reference, data from the Goropu Metabasalt and the Kutu Volcanics (Smith, 2013), the Emo Metamorphics (Worthing and Crawford, 1996), and the Poya Terrane in New Caledonia (Cluzel et al., 2001) are shown.

The calc-alkaline Suckling Granite

Trace element data of the Suckling Granite are illustrated in chondrite-normalized REE (Fig. 8a) and multi-element (Fig. S9a) diagrams. The calc-alkaline rocks of the Suckling Granite are characterized by enriched LREE patterns

([Ce/Yb]$_{CN}$ ~ 15-20) and coupled positive Sr (Sr/Sr* ~ 1.2-6.4) and Eu (Eu/Eu* ~ 1.2-1.4) anomalies as well as high Rb, Ba, Ta, Nb, Zr and Hf (Figs. 8a and S9a). In the tectonic classification diagrams after Pearce et al. (1984), the Suckling Granite plots in the 'volcanic arc & syn-collision granite' (Fig. S10a) and in the 'volcanic arc granite' (Fig. S10b) fields.

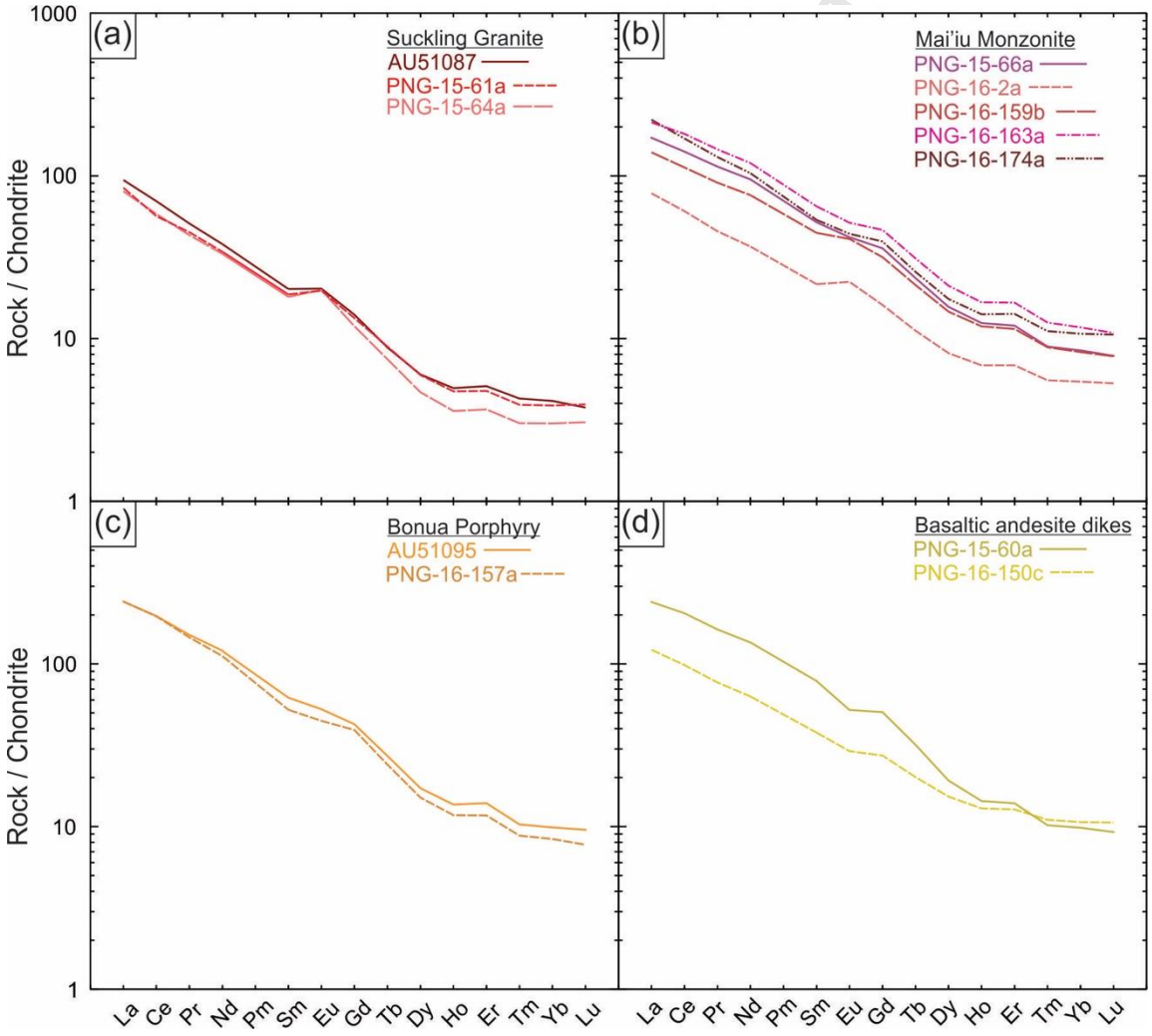

Fig. 8: Chondrite-normalized rare earth element diagrams of the calc-alkaline and high-K suites. Values of Pm were obtained from linear interpolation between Nd and Sm. Normalization values from Arevalo and McDonough (2010) and references therein.

The high-K Mai'iu Monzonite, Bonua Porphyry and basaltic andesite dikes

The high-K Mai'iu Monzonite, Bonua Porphyry and basaltic andesite dikes exhibit similar chondrite-normalized trace element patterns with an enrichment in LREE ($[Ce/Yb]_{CN}$ ~ 10-25, Figs. 8b-d) over HREE and with high Rb, Ba, Ta, Nb, Zr and Hf (Figs. S9b-d). Overall, the trace element patterns resemble those of the Suckling Granite, but most samples lack positive Eu anomalies (Figs. 8b-d). Sr anomalies are variably positive in samples of the Mai'iu Monzonite and Bonua Porphyry (Sr/Sr* ~ 1.0-3.9, Fig. S9b and c). The basaltic andesite dikes reveal coupled negative Sr (Sr/Sr* ~ 0.4-0.5) and Eu (Eu/Eu* ~ 0.8-0.9) anomalies (Figs. 8d and S9d). Trace element abundances are generally higher in the high-K than in the calc-alkaline rocks. In the tectonic classification diagrams after Pearce et al. (1984), the Mai'iu Monzonite, Bonua Porphyry and the basaltic andesite dikes plot in the 'volcanic arc & syn-collision granite' (Fig. S10a) and in the 'volcanic arc granite' (Fig. S10b) fields.

3.3 Zircon U–Pb geochronology

Bonenau Schist/Goropu Metabasalt

Metasedimentary rocks (Bonenau Schist of Smith and Davies, 1976) locally occur intercalated with the Goropu Metabasalt (Fig. 3). Zircons in the Bonenau

Schist are relatively sparse (tens of zircons from samples of ~5 [PNG-16-1153a] and ~20 [PNG-15-18c] kg). Zircons in interbeds of pelitic schist (samples PNG-15-18c, PNG-16-1153a) include both larger (100-250 μm), euhedral zircons with higher aspect ratios (typically ≥2:1) and smaller (generally <150 μm) subrounded zircons with lower aspect ratios (≤2:1); the latter are inferred to be detrital in origin. In PNG-15-18c, zircons yielded exclusively Cretaceous $^{206}Pb/^{238}U$ dates between 111.0 ± 3.1 and 93.6 ± 2.0 Ma and one of 144.6 ± 5.3 Ma (Fig. 9a, Table S1). Nine of 12 U–Pb analyses are ≤10% discordant (Table S1). The Tera-Wasserburg lower-intercept age is 103.3 ± 3.8/5.6 Ma (Fig. 9a, Table 3). Although five zircons in sample PNG-16-1153a yielded $^{206}Pb/^{238}U$ dates of ~3.5-0.2 Ma (24-96% discordant, not shown), 23 of 32 U–Pb analyses (19 of which are ≤10% discordant) yielded dates between 115.8 ± 2.5 and 70.5 ± 2.5 Ma (Fig. 9b; Table S1). Five $^{206}Pb/^{238}U$ dates cluster between 72.9 ± 1.4 and 70.5 ± 2.5 Ma and are statistically distinct from an older group (~116-94 Ma, Fig. 9b). Finally, we obtained a concordant $^{206}Pb/^{238}U$ date of 234.9 ± 3.9 Ma and a discordant one of 1556 ± 21 Ma ($^{207}Pb/^{206}Pb$ = 1615 ± 32 Ma) from the same sample (Fig. 9b, Table S1). The Tera-Wasserburg lower-intercept age of the youngest subpopulation is 71.8 ± 1.5/3.2 Ma (Fig. 9b, Table 3).

Table 3: Resolved zircon U-Pb ages.

Map Unit	Sample	Sample type	Th/U	10th percentile[a]	90th percentile[a]	Age [Ma]	95% [Ma][b]	95% [Ma][c]	95% [Ma][d]	MSWD	n_a / n / n_{zrn}
Bonenau Schist	PNG-15-18c	outcrop				103.3*	0.9	3.8	5.6	16	11/12/11
	PNG-16-1153a	outcrop				71.8*	1.4	1.5	3.2	1.3	5/32/31
Yau Igneous Complex	PNG-15-41bT2	float	3.62	56.7	60.1	58.0*	0.2	0.3	2.3	3.6	50/50/50
	PNG-15-54bT2	clast	0.95	55.5	58.8	56.6*	0.2	0.4	2.3	3.6	50/50/50
	PNG-15-54cT2	clast	1.16	58.4	63.8	60.4*	0.2	0.5	2.5	9.1	51/51/50
	PNG-16-156a	clast	3.40	56.2	60.2	57.8*	0.2	0.5	2.4	9.6	40/41/41
	PNG-16-1008a	outcrop	1.76	56.7	63.4	58.6**	0.2	0.6	2.4	9.1	49/51/50
Suckling Granite	AU51087	float	0.85	3.3	3.6	3.3**	0.02	0.02	0.1	2.4	51/54/49
	AU51088	float	1.17	3.3	4.0	3.3*	0.02	0.04	0.1	3.5	48/50/49
	AU51089	float	0.98	3.4	3.7	3.3*	0.02	0.05	0.1	5.1	44/59/48
	PNG-15-61a	outcrop	0.55	3.8	4.1	3.7**	0.02	0.04	0.2	3.3	65/90/79
	PNG-15-64a	outcrop	0.78	3.6	3.9	3.6**	0.02	0.03	0.1	4.5	82/91/85
Mai'iu Monzonite	PNG-15-66a	outcrop	1.13	2.0	2.3	2.0**	0.02	0.04	0.1	5.4	44/45/43
	PNG-16-2a	outcrop	1.56	2.1	3.2	2.0**	0.02	0.05	0.1	7.6	33/52/49
	PNG-16-159b	outcrop	0.99	3.1	4.0	2.9**	0.04	0.12	0.2	7.1	42/50/50
	PNG-16-163a	outcrop	0.97	2.1	3.1	2.0**	0.03	0.08	0.1	6.2	45/56/50
Bonua Porhyry	PNG-16-157a	outcrop	1.07	2.7	3.8	3.4**	0.02	0.07	0.2	8.8	41/53/53

Sample type: 'clast' refers to gabbroic-tonalitic clast in the Gwoira Conglomerate whereas 'float' refers to stream boulder.

[a]: 10th and 90th percentile of main age population ($^{206}Pb/^{238}U$ dates). See text for definition of main age population.

[b]: 95% uncertainty without overdispersion (Vermeesch, 2018).

[c]: 95% uncertainty with overdispersion (Vermeesch, 2018).

[d]: 95% uncertainty with overdispersion including systematic uncertainties from decay constants (λ_{238}, λ_{235}; Jaffey et al., 1971), $^{238}U/^{235}U$ of GJ-1 (Hiess et al., 2012) and 4% long-term reproducibility of secondary standard zircon Plešovice.

*: Th/U_{magma} = 3 inferred for ^{230}Th correction.

**: Th/U_{magma} from whole-rock composition (Table 2).

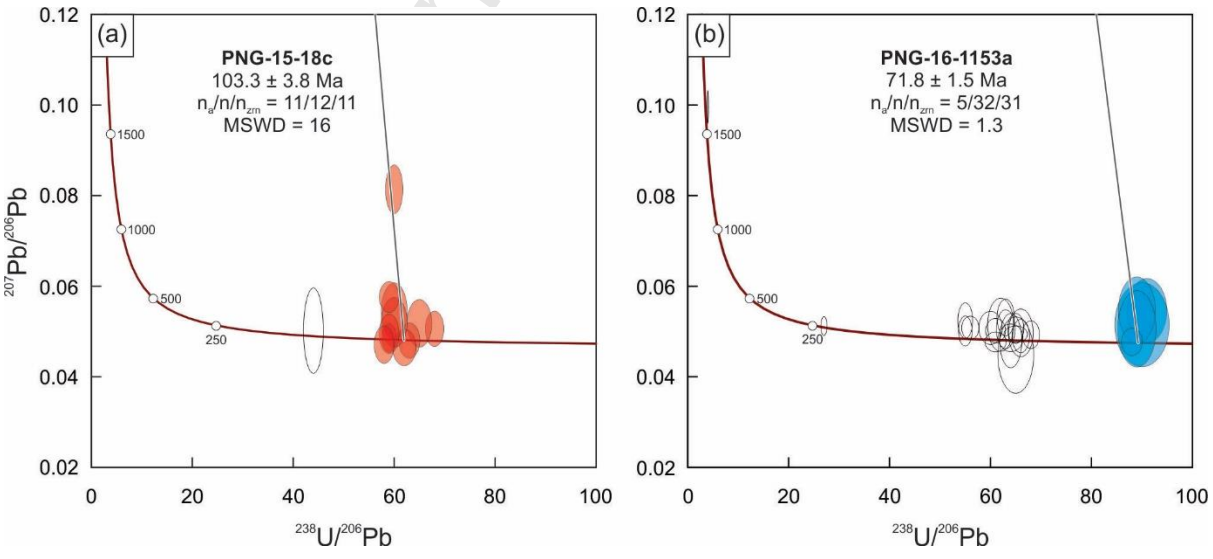

Fig. 9: Tera-Wasserburg diagrams of U–Pb analyses from the Bonenau Schist. Colored and empty ellipses represent U–Pb analyses included and excluded from the calculation of the lower-intercept age, respectively. Uncertainties are given at the

95% confidence interval with overdispersion (Vermeesch, 2018; Table 3). For the calculation of the lower intercept, the upper intercept was anchored at $^{207}Pb/^{206}Pb$ = 0.83. n_a – number of analyses used to calculate the age; n – number of analyses; n_{zrn} – number of zircons analyzed.

Yau Igneous Complex

Zircons were extracted from five Yau Igneous Complex samples: one from an *in situ* tonalite outcrop (PNG-16-1008a), three from gabbroic clasts (PNG-15-54bT2, PNG-15-54cT2, PNG-16-156a) in the Gwoira Conglomerate, and one from a gabbroic boulder (PNG-15-41bT2) in a stream on the hanging wall north of the Mai'iu Fault (Fig. 3). Petrographically, zircon was observed at grain boundaries (plagioclase/amphibole and quartz/plagioclase), at the tip of a sealed fracture(?) in quartz, in altered amphibole and plagioclase, and in a mesostasis consisting mostly of pumpellyite and amphibole (Figs. S11a-n). The zircons are generally prismatic, often present as fragments (broken during the mineral separation?), and orange-pink in color. Most zircons of the Yau Igneous Complex have U and Th contents that fall within the range of 100-800 and 100-2400 ppm, respectively. Mean Th/U values of the individual samples range from 0.95 ± 0.29 to 3.62 ± 2.50 (2s; Table 3).

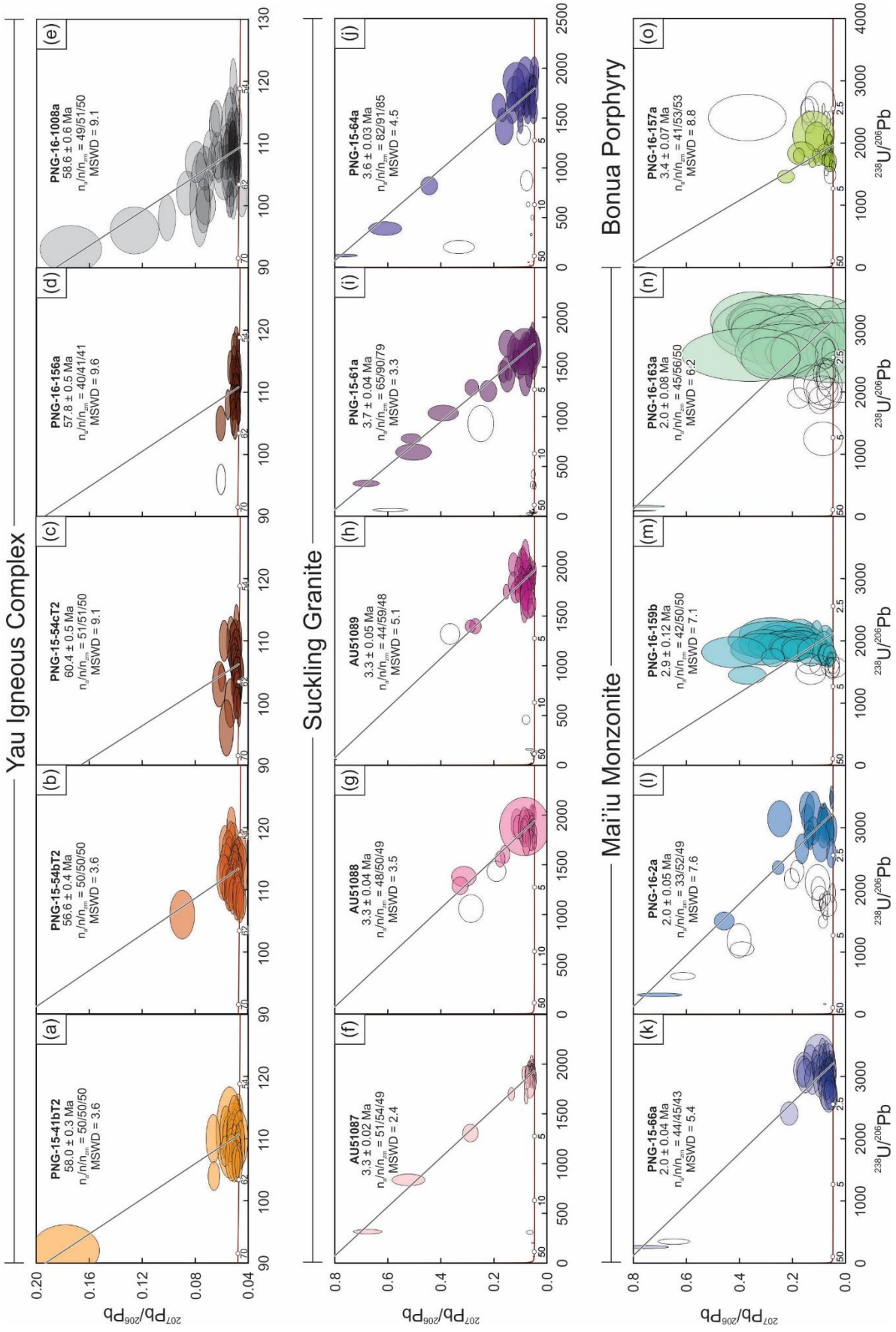
Yau Igneous Complex
Suckling Granite
Mai'iu Monzonite
Bonua Porphyry
(a)
PNG-15-41bT2
58.0 ± 0.3 Ma
n/n = 50/50/50
MSWD = 3.6
(b)
PNG-15-54bT2
56.6 ± 0.4 Ma
n/n = 50/50/50
MSWD = 3.6
(c)
PNG-15-54cT2
60.4 ± 0.5 Ma
n/n = 51/51/50
MSWD = 9.1
(d)
PNG-16-156a
57.8 ± 0.5 Ma
n/n = 40/41/41
MSWD = 9.6
(e)
PNG-16-1008a
58.6 ± 0.6 Ma
n/n = 49/51/50
MSWD = 9.1
(f)
AU51087
3.3 ± 0.02 Ma
n/n = 51/54/49
MSWD = 2.4
(g)
AU51088
3.3 ± 0.04 Ma
n/n = 48/50/49
MSWD = 3.5
(h)
AU51089
3.3 ± 0.05 Ma
n/n = 44/59/48
MSWD = 5.1
(i)
PNG-15-61a
3.7 ± 0.04 Ma
n/n = 65/90/79
MSWD = 3.3
(j)
PNG-15-64a
3.6 ± 0.03 Ma
n/n = 82/91/85
MSWD = 4.5
(k)
PNG-15-66a
2.0 ± 0.04 Ma
n/n = 44/45/43
MSWD = 5.4
(l)
PNG-16-2a
2.0 ± 0.05 Ma
n/n = 33/52/49
MSWD = 7.6
(m)
PNG-16-159b
2.9 ± 0.12 Ma
n/n = 42/50/50
MSWD = 7.1
(n)
PNG-16-163a
2.0 ± 0.08 Ma
n/n = 45/56/50
MSWD = 6.2
(o)
PNG-16-157a
3.4 ± 0.07 Ma
n/n = 41/53/53
MSWD = 8.8
207Pb/206Pb
238U/206Pb

Fig. 10: Tera-Wasserburg diagrams of the Yau Igneous Complex (a-e), Suckling Granite (f-j), Mai'iu Monzonite (k-n) and Bonua Porphyry (o). Colored and empty ellipses represent U–Pb analyses included and excluded from the calculation of the lower-intercept age, respectively. Uncertainties are given at the 95% confidence interval with overdispersion (Vermeesch, 2018; Table 3). For the calculation of the lower intercept, the upper intercept was anchored at $^{207}Pb/^{206}Pb = 0.83$. n_a – number of analyses used to calculate the age; n – number of analyses; n_{zrn} – number of zircons analyzed.

Tera-Wasserburg diagrams of all five samples of the Yau Igneous Complex indicate that zircon U–Pb analyses are generally concordant, or nearly so (Figs. 10a-e); the majority of U–Pb analyses (196 of 243) are ≤10% discordant (Table S1). With the exception of a few highly discordant $^{206}Pb/^{238}U$ analyses (>50% discordance), all others yielded $^{206}Pb/^{238}U$ dates (239 of 243) between 67.1 ± 2.5 and 53.6 ± 1.2 Ma (Table S1). KDE diagrams of four samples of the Yau Igneous Complex reveal that they are defined by a single peak (Figs. S12a-d), although of different breadth and shape. Only in case of PNG-16-1008a does a minor fraction of the $^{206}Pb/^{238}U$ dates form a secondary KDE peak on the older tail (Fig. S12e). Because these slightly older U–Pb analyses intersect the discordia in the Tera-Wasserburg diagram (Fig. 10e), they are considered for the calculation of the lower-intercept age. Of the four samples defined by a single KDE peak, 80% of the $^{206}Pb/^{238}U$ dates span intra-sample age ranges of ~3-5 myr; in the case of PNG-16-1008a it is ~7 myr (Table 3). A CAD diagram of the Yau Igneous Complex samples reveals relatively sigmoidal-like topologies of the $^{206}Pb/^{238}U$ dates of each sample in the 70-50-Ma age range;

note, however, the slight change in slope of the CAD at ~75% of PNG-16-1008a compared to the other samples (Fig. S13a). Lower-intercept ages of the five samples range from 60.4 ± 0.5/2.5 to 56.6 ± 0.4/2.3 Ma (Figs. 10a-e, Table 3).

Suckling Granite

Zircons were separated from five samples of the Suckling Granite. The zircons occur within plagioclase, K-feldspar, quartz and biotite crystals and at the grain boundaries between amphibole and plagioclase (Figs. S11o-s). The grains are typically prismatic, euhedral, pink, translucent, have an average size of 100-200 µm and aspect ratios of 2:1 to 3:1. Cathodoluminescence (CL) images of two Suckling Granite samples (PNG-15-61a, PNG-15-64a) reveal numerous zircons with xenocrystic cores (moderate-high CL intensities, low-high contrast) mainly enclosed by rims with oscillatory zoning (low-moderate CL intensities, low-intermediate contrast), but sector, stripy, diffuse, patchy and complex zoning patterns have also been observed in these samples (Fig. 11a). Most zircons of the Suckling Granite have U and Th contents that fall within the range of 200-1500 and 100-1400 ppm, respectively. Mean Th/U values of the individual samples range from 0.55 ± 0.81 to 1.17 ± 1.71 (2s; Table 3).

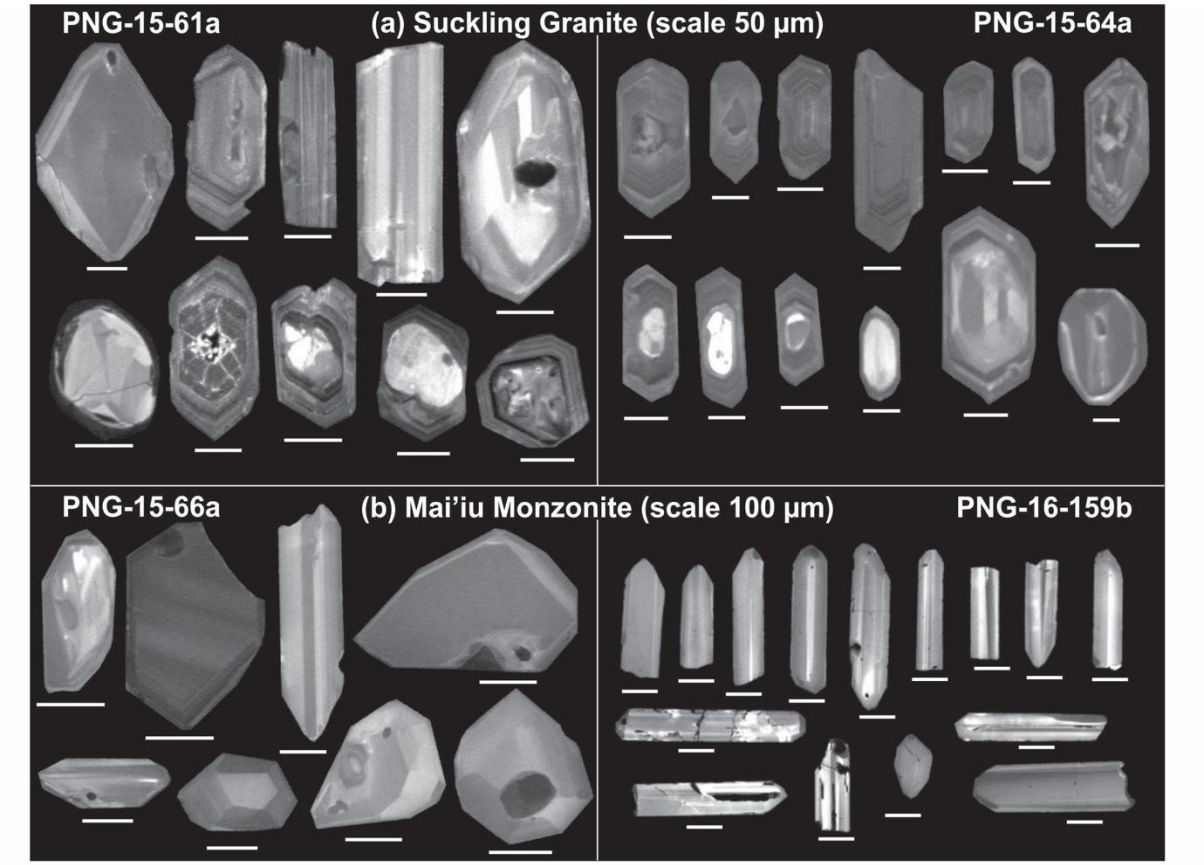

Fig. 11: Cathodoluminescence (CL) images of zircon from the (a) Suckling Granite (PNG-15-61a, PNG-15-64a) and (b) Mai'iu Monzonite (PNG-15-66a, PNG-16-159b).

Tera-Wasserburg diagrams of all five samples of the Suckling Granite reveal that the majority of zircon U–Pb analyses are discordant (Figs. 10f-j); only 78 of 343 U–Pb analyses are ≤10% discordant (Table S1). $^{206}Pb/^{238}U$ dates of the Suckling Granite range from 1795 ± 58 ($^{207}Pb/^{206}Pb$ = 1633 ± 38 Ma) to 1.9 ± 0.2 Ma, but 282 of the 343 dates fall into the 5-3-Ma age range (Table S1). KDE diagrams of the five samples of the Suckling Granite exhibit essentially unimodal age distributions with a few $^{206}Pb/^{238}U$ dates forming tails on the older side, and in one instance (PNG-15-61a), a subtle peak on the younger side (Figs. S12f-j). While the three youngest U–Pb analyses of PNG-15-61a are discarded from the calculation due to low signal-to-

noise ratios, those that are slightly older and intersect the discordia in the Tera-Wasserburg diagrams are considered for the calculation of the lower-intercept age (Figs. 10f-j). Eighty percent of the $^{206}Pb/^{238}U$ dates <10 Ma span intra-sample age ranges of ~0.3-0.7 myr (Table 3). A CAD diagram reveals relatively sigmoidal-like topologies of the $^{206}Pb/^{238}U$ dates of each of the five samples in the 8-1-Ma age range (Fig. S13b); note, however, the relatively big step between the three youngest and older dates of PNG-15-61a. Lower-intercept ages of the five samples range from 3.7 ± 0.03/0.2 to 3.3 ± 0.05/0.1 Ma (Figs. 10f-j, Table 3). Among these five samples are two (AU51088, AU51089) that were previously dated by Davies and Smith (1974) using K–Ar methodology (their samples 6552-2577 and 6552-2578). The lower-intercept zircon U–Pb ages of these samples (both 3.3 ± 0.1 Ma, Figs. 10g and h) are significantly younger than their apparent hornblende K–Ar ages (9.4 ± 0.8 and 10.8 ± 0.8 Ma), but essentially identical to their biotite K–Ar age (3.3 ± 0.1 Ma). Twenty-one concordant U–Pb analyses of the Suckling Granite samples yield $^{206}Pb/^{238}U$ dates between 1089 ± 27 ($^{207}Pb/^{206}Pb$ = 1036 ± 23 Ma) and 15.2 ± 1.3 Ma (Table S1).

Mai'iu Monzonite

The plutonic Mai'iu Monzonite samples (Fig. 3; PNG-15-66a, PNG-16-159b, PNG-16-163a) yielded large volumes of zircon (>1-3 grams for rock samples of ~5-10 kg each) despite the significantly more mafic composition of these rocks. Conversely, the zircon yield of a ~1-m-wide dike of Mai'iu Monzonite (Fig. 3; PNG-16-2a) was significantly less (<100 crystals). Zircon was identified as inclusions in

hornblende, plagioclase, biotite, K-feldspar and quartz, as well as at grain boundaries (Figs. S11t-x).

The zircons are typically euhedral, pink and translucent. Two Mai'iu Monzonite samples (PNG-15-66a, PNG-16-163a) exhibit a variety of morphologies (stubby, long-prismatic, platy, equant), sizes (50-500 μm) and aspect ratios (1:1 to 5:1), while those of PNG-16-159b are dominantly prismatic and typically have higher aspect ratios (generally >2:1 to 6:1). CL images of zircons from two samples (PNG-15-66a, PNG-16-159b) reveal that most grains show faint stripy, sector or diffuse zoning, but some are virtually unzoned, and a few have rare faint oscillatory zoning (Fig. 11b). Rare xenocrystic cores were observed. A common feature is the occurrence of CL-dark mineral inclusions of unknown composition in zircons of these samples. Most zircons of the Mai'iu Monzonite have U and Th contents that fall within the range of 50-900 and 50-1400 ppm, respectively. Mean Th/U values of the individual samples range from 0.97 ± 0.70 to 1.56 ± 1.81 (2s; Table 3).

Tera-Wasserburg diagrams of all four samples of the Mai'iu Monzonite reveal that the majority of zircon U–Pb analyses are discordant (Figs. 10k-n); only 19 of 203 U–Pb analyses are ≤10% discordant (Table S1). $^{206}Pb/^{238}U$ dates of the Mai'iu Monzonite range from 542 ± 15 to 1.8 ± 0.1 Ma, but 190 of the 203 dates are <5 Ma (Table S1). KDE diagrams of the four Mai'iu Monzonite samples reveal age spectra with a main peak and, except PNG-15-66a, obvious shoulders or tails on the older sides (Figs. S12k-n). Those U–Pb analyses that are slightly older and intersect the discordia in the Tera-Wasserburg diagrams (Figs. 10k-n) are considered for the calculation of the lower-intercept age. Eighty percent of the $^{206}Pb/^{238}U$ dates <10 Ma

span intra-sample age ranges of ~0.4-1.2 myr (Table 3). A CAD diagram reveals that the topologies of $^{206}Pb/^{238}U$ dates of three samples of the Mai'iu Monzonite (PNG-16-2a, PNG-16-159b, PNG-16-163a) have clear inflections points (i.e., change in slope) in the 7-1-Ma age range (Fig. S13c); this is particularly obvious in sample PNG-16-2a. Only PNG-15-66a exhibits a relatively sigmoidal-like topology (Fig. S13c). Lower-intercept ages of the four samples range from 2.9 ± 0.12/0.2 to 2.0 ± 0.08/0.1 Ma (Figs. 10k-n, Table 3). Two concordant U–Pb analyses of the Mai'iu Monzonite dike PNG-16-2a yield $^{206}Pb/^{238}U$ dates of 542 ± 15 and 514 ± 11 Ma (Table S1).

Bonua Porphyry

Zircons in a sample of the Bonua Porphyry (PNG-16-157a, Fig. 3) were identified in thin section at phase boundaries between biotite and K-feldspar; and between prehnite(?) and K-feldspar. The zircons are generally pink, translucent and range in size from 100 to 400 µm. They are typically prismatic, but some are smoothly rounded. Zircons are less abundant in this sample of the Bonua Porphyry compared to those from the Suckling Granite and Mai'iu Monzonite. Most zircons of the Bonua Porphyry have U and Th contents that fall within the range of 100-1400 and 100-1800 ppm, respectively. An average Th/U of 1.07 ± 1.63 (2s) was calculated (Table 3).

A Tera-Wasserburg diagram of the Bonua Porphyry sample reveals that the majority of zircon U–Pb analyses are discordant (Fig. 10o); only 9 of 53 U–Pb analyses are ≤10% discordant (Table S1). $^{206}Pb/^{238}U$ dates of this sample range

from 1061 ± 110 ($^{207}Pb/^{206}Pb$ = 4900 ± 17 Ma) to 2.5 ± 0.3 Ma, but 49 of the 53 dates are <5 Ma (Table S1). A KDE diagram reveals a bimodal age spectrum with a main peak at ~3.7 Ma and a secondary peak at ~2.6 Ma. Most of these younger U–Pb analyses have low signal-to-noise ratios and are discarded from the calculation of the lower-intercept age; and so are the analyses on the older tail of the main peak that do not intersect the discordia (Fig. 10o). Eighty percent of the $^{206}Pb/^{238}U$ dates <10 Ma span an age range of ~1.1 myr (Table 3). A CAD diagram reveals a sigmoidal-like topology of the $^{206}Pb/^{238}U$ dates of this sample, but with a relatively large step (compared to the others of this sample) between ~2.8 and ~3.0 Ma in the 7-1-Ma age range (Fig. S13c). The lower-intercept age of this sample is 3.4 ± 0.07/0.2 Ma (Fig. 10o, Table 3). Two concordant U–Pb analyses yield $^{206}Pb/^{238}U$ dates of 105.7 ± 3.0 and 96.6 ± 5.3 Ma (Table S1).

Basaltic andesite dike

Two zircon crystals were separated (from ~30 kg of rock) from one of the two basaltic andesite samples (PNG-15-60a, Fig. 3) near the trace of the Mai'iu Fault. Morphologically, one grain was euhedral (U = 246 ppm, Th = 274 ppm) and the other rounded (U = 241 ppm, Th = 215 ppm). The euhedral and rounded grains yielded $^{206}Pb/^{238}U$ dates of 0.7 ± 0.1 and 89.9 ± 2.2 Ma, respectively (Table S1).

Modern stream sediments

Modern stream sediments were collected in the Mai'iu and Bonua Rivers. Both streams drain Mt. Suckling: the Mai'iu River (PNG-15-76d) to the north, and the Bonua River (PNG-16-157b) to the south (Fig. 3). Zircons in these stream sediments are generally euhedral, pink and translucent. $^{206}Pb/^{238}U$ dates of the detrital zircons from the Mai'iu River (PNG-15-76d) range from 701 ± 23 to 1.6 ± 0.4 Ma (Table S1). Only 51 of 301 are ≤10% discordant. A KDE diagram reveals that the $^{206}Pb/^{238}U$ dates of the Mai'iu River sample form a single peak with a shoulder on the younger side (Fig. 12a). Eighty percent of the $^{206}Pb/^{238}U$ dates <10 Ma range between ~4.4 and ~2.2 Ma (Table S1). Only 20 of 301 analyses yielded dates >10 Ma, most of which are discordant (Table S1). Three concordant analyses on two grains yield Jurassic (197.2 ± 4.8 and 186.7 ± 4.3 Ma) and Cretaceous (114.3 ± 2.9 Ma) $^{206}Pb/^{238}U$ dates (Table S1).

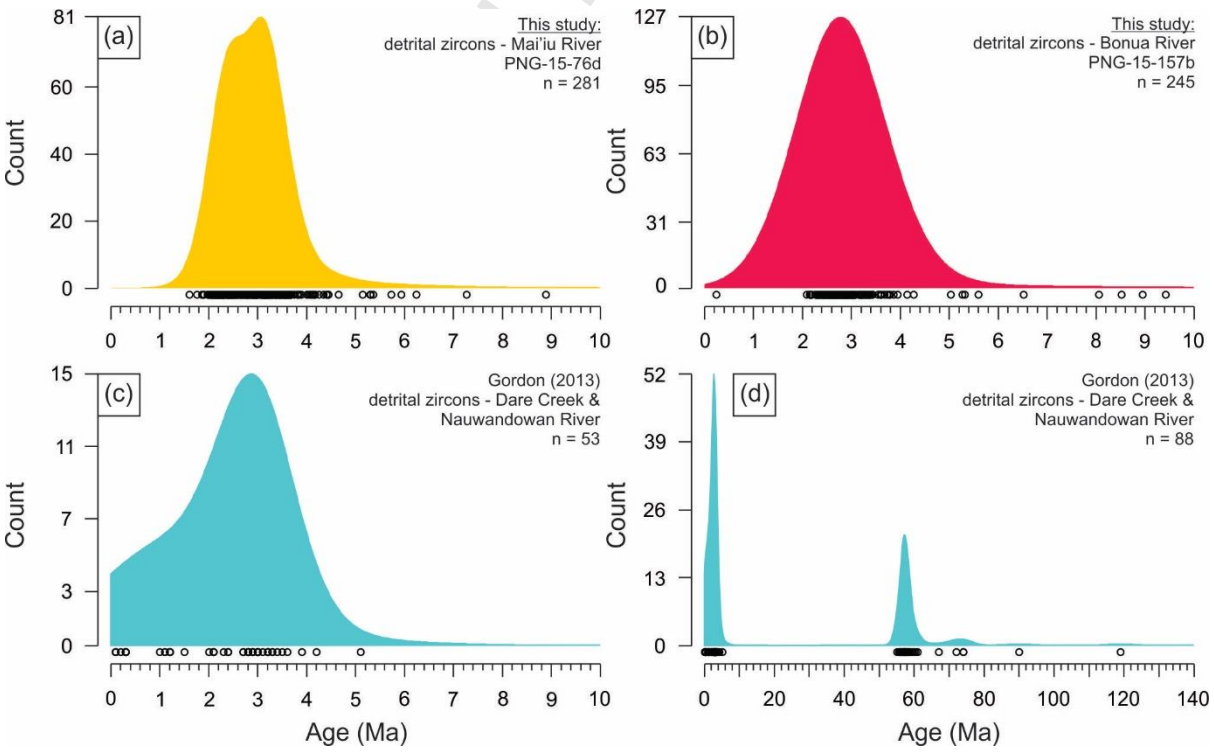

Fig. 12: Adaptive kernel density estimation (KDE) diagrams of $^{206}Pb/^{238}U$ dates of detrital zircon from streams draining the Suckling-Dayman metamorphic core

complex. Detrital zircons from the Mai'iu (a) and Bonua (b) Rivers are from this study. Detrital zircons from the Nauwandowan River and Dare Creek (c-d) are from Gordon (2013). Plots (c) and (d) show 0-10 and 0-140 Ma time windows of the same dataset, respectively. Note, $^{206}Pb/^{238}U$ dates reported by Gordon (2013) are corrected for Pb_c. The bin widths of the histograms (not shown) of plots a-c were set to 0.5 myr, and to 5 myr for plot d.

$^{206}Pb/^{238}U$ dates of zircons from the Bonua River sample PNG-16-157b range from 2034 ± 86 ($^{207}Pb/^{206}Pb$ = 4852 ± 56 Ma) to 0.2 ± 0.1 Ma (Table S1). Only 49 of 257 are ≤10% discordant. A KDE diagram reveals that the $^{206}Pb/^{238}U$ dates of the Bonua River sample form a single peak with no shoulders or secondary peaks (Fig. 12b). Eighty percent of the $^{206}Pb/^{238}U$ dates <10 Ma range between ~3.8 and ~2.4 Ma (Table S1). Only 12 of 257 analyses yielded dates >10 Ma, of which all are discordant (Table S1).

4. Discussion

4.1 The Goropu Metabasalt and its tectonic implications

The Goropu Metabasalt has geochemical affinities transitional between N-MORB and E-MORB, but closer to the latter (i.e., $[Ce/Yb]_{CN} > 1$). Its close spatial association (Fig. 3) and geochemical similarity (Fig. 7) to the Kutu Volcanics supports the view that both units have a common origin (e.g., Smith, 2013). We have

here constrained the maximum age of the Goropu Metabasalt from the U–Pb ages of zircons, interpreted as of detrital nature, in metasedimentary intercalations of the Bonenau Schist. The youngest concordant subpopulations (from samples PNG-15-18c and PNG-16-1153a) yield ages of 103.3 ± 2.7/4.9 and 71.8 ± 1.1/3.1 Ma, respectively, that provide maximum depositional ages (MDA). The five youngest $^{206}Pb/^{238}U$ dates of PNG-16-1153a (~3.5-0.2 Ma) have no relevance for the determination of the protolith age and are thus not further considered. A rare concordant Late Triassic $^{206}Pb/^{238}U$ date (235 ± 4 Ma) may indicate the presence of early Mesozoic rocks in the source area.

These detrital zircon U–Pb MDAs support the biostratigraphy-based inference of a Late Cretaceous (Maastrichtian) age for the Bonenau Schist as previously reported by Smith and Davies (1976). Our MDAs may suggest formation of Goropu Metabasalt over an extended eruptive period between ~103 and ~72 Ma, although this result is uncertain because of the limited number of U–Pb analyses and samples. If one considers the two MDAs to be meaningful, then a southward younging trend is suggested by the relative positions of the two Bonenau Schist samples. Such southward younging would agree with the overall younging trend implied by the, in part, Eocene age of the unmetamorphosed Kutu Volcanics located to the south of the Late Cretaceous Goropu Metabasalt of the SDMCC (Fig. 3).

The age of the Goropu Metabasalt has implications for paleogeographic reconstructions of the Southwest Pacific region. The Goropu Metabasalt and the Emo Metamorphics in the central Papuan Peninsula occur in the same tectonic position below the Owen Stanley Fault Zone and the PUB (Fig. 1). Although

geochemical data of the Goropu Metabasalt exhibit MORB-only compositions and those from the Emo Metamorphics fall both within and above the MORB-OIB array in Nb/Yb vs. Th/Yb (Fig. 7) and Ta/Yb vs. Th/Yb diagrams, which was argued to indicate contamination by continental crust (Whattam, 2009) or suprasubduction-zone processes (Smith, 2013), we regard them as lateral equivalents. Both the Goropu Metabasalt and the Emo Metamorphics have been considered to be remnants of a back-arc basin (Worthing and Crawford, 1996) that opened in the Late Cretaceous to the northeast of the Australian continent (Fig. 2). This back-arc basin is, in some models, portrayed as the lateral extension of a much larger system that includes the South Loyalty and East New Caledonia Basins (Cluzel et al., 2001; Eissen et al., 1998; Whattam, 2009).

The Papuan Peninsula and New Caledonia share striking similarities with regard to their tectonic history (as summarized by Little et al., 2019) including (1) the Paleocene-Eocene initiation of ophiolite obduction (Peridotite Nappe in New Caledonia at ~56 Ma vs. ~58 Ma for the PUB); (2) intrusion of Early Eocene (50–55 Ma) suprasubduction-zone dikes and plutons into the ophiolitic nappes in both places; (3) emplacement of the ophiolitic rocks over an allochthon of mostly Late Cretaceous, MORB-affinity marginal basin rocks (Poya Terrane in New Caledonia; Goropu-Kutu in PNG); and (4) eventual clogging of that subduction zone during the Late Eocene–Oligocene by attempted subduction of a continental plateau of mostly Cretaceous-age rocks (Norfolk Ridge in New Caledonia; Papuan Peninsula in PNG). In addition, geochemical data from the Goropu Metabasalt and Kutu Volcanics in PNG are very similar to those from the Poya Terrane in New Caledonia, although the latter also includes OIB-type rocks (Fig. 7). These commonalities between the

Papuan Peninsula and New Caledonia support the existence of an extensive back-arc basin system between the Australian continent in the southwest and the Southwest Pacific in the northwest during the Late Cretaceous-Paleogene.

A recent study from the Solomon Islands reported xenocrystic zircon U–Pb ages that indicate derivation from the northeastern Gondwana margin (Tapster et al., 2014), a result that has been taken to suggest that the Solomon Island Arc (part of the Melanesian Arc system, Fig. 1b) is not purely intra-oceanic in nature (Seton et al., 2016). Hence, the age of the Goropu Metabasalt may constrain the age of the Emo Basin and the timing of rifting events that separated hyper-extended continental crust from the northeastern margin of Gondwana.

4.2 Tectonic setting and relevance of the Yau Igneous Complex

Petrogenesis

The broad range of SiO_2 contents of the dolerites, quartz-gabbros and tonalites of the Yau Igneous Complex (~45-63 wt%) suggests that this unit is internally differentiated, a conclusion already drawn by Smith and Davies (1976) on petrographic grounds. Compositionally, the virtual absence of Fe-Ti oxides in the dolerites, their higher MgO, Cr and Ni contents compared to the gabbroic-tonalitic rocks (Table 2), slightly enriched chondrite-normalized LREE patterns (Fig. 6), and the resemblance and (in some cases) overlap with “canonical” MORB values of Ti/Eu, Y/Ho and Ce/Pb from the literature (Table 4) collectively suggest that these

rocks formed in a MORB environment, transitional between E- and N-MORB (Fig. 7). The close match of the elemental patterns of the dolerites and the Goropu Metabasalt (Figs. 6 and S8) further supports this notion.

Table 4: Trace element characteristics of the Yau Igneous Complex

Sample	Ti/Eu	Y/Ho	Ce/Pb	MgO [wt%]	Cr [ppm]	Ni [ppm]
Low-silica suite:						
PNG-15-3b	7580	23.6	32.9	7.83	301	67
PNG-15-4a	6923	24.3	65.3	6.74	191	79
PNG-16-156a	6782	25.3	124.4	4.02	2	28
PNG-16-1029a	7697	24.8	38.8	3.30	9	16
High-silica suite:						
AU51082	2102	25.0	219.5	1.47	2	bdl
PNG-16-108b	2536	25.1	278.0	1.62	1	bdl
PNG-16-1008a	1372	25.9	90.7	0.91	5	bdl
MORB - Arevalo and McDonough (2010)	7060 ± 1270*	28.4 ± 3.6*	22.2 ± 9.7*	7.69 ± 2.40*	326 ± 183*	200

*: Uncertainties at the 2s confidence level.

bld: below detection limit

The quartz-gabbro and tonalites of the high-silica suite of the Yau Igneous Complex are more fractionated than the dolerites. The low MgO (0.91-1.62 wt%, Table 2), the 5-6 order-of-magnitude difference in elemental abundances between compatible and incompatible elements (Fig. S8b), the negative Eu, Ti and V (Figs. 6 and S8b) and Sr anomalies, as well as the very low Cr and Ni contents (Table 4), are those expected from more evolved melts (compared to the dolerites). The coupled negative Ti and V anomalies suggest fractionation by Fe-Ti oxides and the coupled negative Eu and Sr anomalies may indicate plagioclase fractionation. The fact that the REE patterns of the dolerites of the low-silica suite and the quartz-gabbro and tonalites of the high-silica suite are subparallel to each other may imply that they are linked by crystal fractionation. By contrast, the chondrite-normalized REE patterns of

the quartz-gabbro and tonalite of the low-silica suite are depleted. This contrasts with the slightly enriched patterns of the Goropu Metabasalt.

The age of the Yau Igneous Complex

Zircon U–Pb analyses of five samples of quartz-gabbros and tonalites of the Yau Igneous Complex each reveal a large range of $^{206}Pb/^{238}U$ dates of at least ~4 myr. Such apparently protracted crystallization durations are not compatible with the idea that zircon in mafic/tholeiitic rocks formed in late-stage, fractionated melt pockets (Schaltegger and Davies, 2017). In both fast- and slow-spreading mid-ocean ridge settings, time scales of zircon crystallization in oceanic gabbroic plutons were found to be on the order of ~0.1-0.2 myr (Lissenberg et al., 2009; Rioux et al., 2012), significantly shorter than the span of zircon crystallization we observe in the quartz-gabbros and tonalites of the Yau Igneous Complex. The reason for these apparently protracted time scales of zircon growth in the samples of the Yau Igneous Complex remains obscure, but may be due to inheritance or post-crystallization processes that affected the zircons in this unit. Despite the broad range of $^{206}Pb/^{238}U$ dates, KDE (Figs. S12a-e) and CAD (Fig. S13a) diagrams exhibit rather coherent age populations. Future CL imaging and *in-situ* dating of zircons in its petrologic context may elucidate the cause of this broad range of $^{206}Pb/^{238}U$ dates in the Yau Igneous Complex.

The Yau Gabbro (Yau Igneous Complex of this study) was previously described as a subvolcanic pluton related to the Goropu Metabasalt (Smith and

Davies, 1976). Tera-Wasserburg zircon U–Pb lower-intercept ages of the Yau Igneous Complex ranging between ~60 and ~57 Ma (Figs. 10a-e) suggest crystallization in the Paleocene. The U–Pb ages for these intrusions post-date the Late Cretaceous Goropu Metabasalt by at least ~5-10 myr, thereby providing a minimum age for eruption of the Goropu lavas. Interestingly, the Paleocene (~60-57 Ma) U–Pb crystallization ages of the Yau Igneous Complex overlap with the inferred timing of southwest-directed obduction of the PUB over the rifted Australian margin at 58.3 ± 0.4 Ma, and also with magmatic activity in the CVA between ~59 and ~47 Ma (Lus et al., 2004; Rogerson et al., 1991; Walker and McDougall, 1982). A common origin of the Yau Igneous Complex and the igneous rocks of the CVA is, however, unlikely given the MORB-like character of the former and the arc-like affinities of the latter; and their occurrence on opposite sides of the Owen Stanley Fault, which is the inferred subduction thrust.

4.3 The syn-extensional intrusions and their bearing on Mai'iu Fault inception and crustal structure of the SDMCC

Petrogenesis

Based on mineralogical differences and major oxide compositions, calc-alkaline (Suckling Granite) and high-K (Mai'iu Monzonite, Bonua Porphyry, basaltic andesite dikes) suites may be distinguished. We observe a transition from felsic/peraluminous bulk compositions (Suckling Granite) at ~3.7-3.6 Ma to intermediate-mafic/metaluminous ones (Mai'iu Monzonite, Bonua Porphyry) at ~3.4-

2.0 Ma (Fig. S6). Associated with this was an accompanying change in mineralogy (white mica → biotite → biotite + hornblende). This trend may record an increase in the melting of more primitive infracrustal (I-type) material over time, initial partial melting of crustal (S-type) material, or a combination of both. This trend we observe is consistent with Chappell and White's (1974) inference that S-type granites tend to form early in the intrusive sequence relative to I-types.

We infer that the Suckling Granite was derived by partial melting of underlying Australian-derived continental crust. This inference is supported by the coupled positive Eu (Eu/Eu* = 1.2-1.4) and Sr (Sr/Sr* = 1.2-6.4) anomalies in the samples of the Suckling Granite (possibly through incorporation of plagioclase) and the occurrence of xenocrystic zircons of Precambrian to Cenozoic age in the granitoids. Little et al. (2019) inferred that Australian-derived sediments deposited on rifted continental margin were subducted along a Miocene thrust below the slab of Goropu Metabasalt-Kutu Volcanics. In this model, the subducted continental crust partially melted at mantle depths after the onset of extension in the Woodlark Rift. These partial melts rose into the extending lithosphere of the overlying rift, locally emerging to form the gneiss domes of the D'Entrecasteaux Islands. In their model, small amounts of melts migrated up the Mai'iu Fault zone where the Suckling Granite and Mai'iu Monzonite were intruded. Alternative scenarios for the formation of the Suckling Granite may involve partial melting of the continental crust that is more nearly beneath the Goropu Metabasalt in response to extension in the Woodlark Rift, decompression, and/or a temperature increase associated with the rifting process.

High-K magmatic rocks are typically linked to subduction (e.g., Morrison, 1980). In the SDMCC, plutons with high-K compositions were intruded at ≤3.4 Ma. This late Pliocene age is synchronous with extension of the continental Woodlark Rift and oceanic Woodlark Basin (Taylor and Huchon, 2002) and post-dates the Miocene subduction zone that was responsible for the HP-UHP metamorphism of the eclogitic rocks in the D'Entrecasteaux Islands (Little et al., 2019; Webb et al., 2014; Zirakparvar et al., 2013). Although transient south-directed subduction of Solomon Sea crust may have occurred at the Trobriand Trough between ~6 and ~2 Ma (Holm et al., 2016), we oppose a causative relationship with respect to the high-K intrusions of the SDMCC. Some have argued (cf. Johnson et al., 1978) that the arc-like chemical signatures of many Late Cenozoic volcanic rocks in PNG (including rocks that have been associated with the Maramuni Arc) were inherited from one or more previous phases of subduction. Based on trace element and volatile abundances (4,500 ppm S; enriched Th/Nb; up to 3.3 wt% H_2O) in olivine-hosted melt inclusions from the Goropu Crater (Fig. 3), Ruprecht et al. (2013) inferred that the basaltic andesite was derived from partial melting of mantle that had previously been affected by subduction, but that low H_2O/Ce values of ~350-800 in the rock are unlike those from active volcanic arcs. Farther west, an isotopic study by Gill et al. (1993) found that lava erupted in 1951 from Mt. Lamington (Figs. S1 and S2) lacked, in contrast to Holocene lavas from the Bismarck Volcanic Arc just north of the active New Britain Trench (Fig. 1b), an enrichment in ^{10}Be, a result that may suggest no addition of recent pelagic sediments in the melt source; or in other words, no recent subduction. This is consistent with seismic and geodetic data that suggest no present-day convergence on either side (Trobriand Trough vs. Aure-Moresby-Pocklington Trough; Fig. 1) of the Papuan Peninsula (Abers et al., 2016; Abers and Roecker,

1991; Drummond et al., 1979; Wallace et al., 2004, 2014). Following Johnson et al. (1978), we suggest that the high-K magmatic rocks in the SDMCC (Mai'iu Monzonite, Bonua Porphyry, basaltic andesite dikes) record an inherited geochemical signature from one or several previous phases of subduction.

Although the calc-alkaline Suckling Granite and the high-K rocks of the Mai'iu Monzonite, Bonua Porphyry and the basaltic andesite dikes formed in the common extensional regime of the Woodlark Rift, the high-K rocks possibly reflect the increasing role of infracrustal melts and/or the decreasing contribution of partial melting of continental material. The latter may be reflected in a polarity reversal of the coupled Sr and Eu anomalies from positive in the Suckling Granite (Eu/Eu* = 1.2-1.4; Sr/Sr* = 1.2-6.4) to negative in the basaltic andesite dikes (Eu/Eu* = 0.8-0.9; Sr/Sr* = 0.4-0.5), the latter representing a younger phase of magmatism. In the Woodlark Rift, a ~250-km-long by <100-km-wide corridor of asthenospheric mantle (V_p/V_p up to -4%; Fig. 1) has been imaged by teleseismic P- and S-waves (Eilon et al., 2015). The presence of this slow region has been attributed to near-complete thermal and chemical erosion of the lithospheric mantle by adiabatic upwelling of asthenospheric mantle ahead of the west-propagating seafloor spreading tip (Abers et al., 2016; Eilon et al., 2015). Daczko et al. (2011) suggested that the mafic dikes at the range front (the basaltic andesite dikes of this study) may have been produced by partial melting of rising asthenosphere.

We argue that the importance of the rising asthenosphere in producing more primitive melts (Mai'iu Monzonite, Bonua Porphyry and the basaltic andesite dikes), compared to the earlier more crustal-like melts of the slightly older Suckling Granite,

has increased since the onset of extension along the Mai'iu Fault (see section 4.3.2). Thermobarometry of olivine (forsterite content >89%) from historic basaltic andesite lava erupted at the Goropu Crater suggests that these magmas equilibrated prior to their extraction from the mantle at temperatures and pressures of ~1150-1200°C and 5.5-7.5 kbar, respectively (Ruprecht et al., 2013). Ruprecht et al. (2013) noted that the thermobarometry-based mantle temperatures are well above the melting point of the exhumed felsic HP-UHP rocks on the D'Entrecasteaux Islands, suggesting that the thermal pulse that led to mantle melting could have been a result of Woodlark Rift propagation in the last several million years. These temperature-pressure constraints seemingly support the inference of an increasing mantle influence on the magmatism in the Woodlark Rift over the last few million years.

The age of the syn-extensional granitoids

Zircons from the granitoids of the Suckling Granite, Mai'iu Monzonite and Bonua Porphyry show characteristics of magmatic growth. This includes: (1) Th/U > 0.1, (2) crystals that are mostly prismatic with pyramidal terminations and (3) crystals that show (where CL images are available) oscillatory, sector and stripy zoning (Corfu et al., 2003; Lancaster et al., 2017; Rubatto et al., 1998; Williams and Claesson, 1987). The Tera-Wasserburg zircon U–Pb lower-intercept ages of the Suckling Granite, Mai'iu Monzonite and Bonua Porphyry (reported in Table 3) that range from ~3.7 to ~2.0 Ma are interpreted as their crystallization ages.

Based on the results presented in Tera-Wasserburg, KDE and CAD diagrams, a small number of U–Pb analyses (empty ellipses in Fig. 10) have been excluded from the age calculation either due to low signal-to-noise ratios, their inferred ante-/xenocrystic nature (cf. Miller et al., 2007), or Pb_c compositions unlike those presented from co-genetic feldspars in the Suckling Granite and Mai'iu Monzonite (Table S2). In particular, we suggest samples of the Mai'iu Monzonite to contain abundant antecrystic zircons (Figs. S12l-n), whereas those of the Suckling Granite (Figs. 10f, h and i) have zircons that clearly pre-date their respective lower-intercept ages and are readily interpreted as xenocrysts. Alternative explanations for the spread of U–Pb dates in the young granitoids include post-magmatic processes such as Pb loss and zircon recrystallization, but these are improbable given the young age of these rocks and the magmatic CL textures, respectively.

The lower-intercept ages of the three Suckling Granite stream boulders (all three ~3.3 Ma, AU51087-AU51089; Table 3) dated in this study are in excellent agreement with the $^{206}Pb/^{238}U$ age of 3.3 ± 0.1 Ma for the Suckling Granite boulder (2*, Fig. 3) reported by Daczko et al. (2011). Our U–Pb data for zircon do not, however, support the hornblende K–Ar dates of ~10.8-4.4 Ma reported by Davies and Smith (1974) for the Suckling Granite and Mai'iu Monzonite (1* and 3*, Fig. 3). We suspect their K–Ar dates were affected by excess Ar (cf. McDougall and Harrison, 1999). The $^{206}Pb/^{238}U$ date of a single euhedral zircon from a basaltic andesite dike (PNG-15-60a) may suggest emplacement at 0.7 ± 0.1 Ma. This is, however, only a first attempt to date the undeformed basaltic andesite dikes exposed in the most recently uplifted parts of the mylonitic Goropu Metabasalt.

The inferred crystallization ages of the uplifted and faulted granitoids near Mt. Suckling place constraints on the timing of activity on the Mai'iu Fault. The mostly massive-textured granitoids are truncated above by the Mai'iu Fault and occur in its footwall. The oldest known granitoid (sample PNG-15-61a of the Suckling Granite) records a progression from magmatic to ductile solid-state deformation (Figs. 4e and S4), suggesting syn-extensional intrusion of this sample at or below the brittle-ductile transition. By inference, the younger granitoids must be syn-extensional too. The massive-textured (unfoliated) microstructure of the younger samples may reflect their intrusion into a cooler, shallower, and more exhumed (i.e., more brittle) part of the footwall. Based on these arguments, we infer that the Mai'iu Fault was initiated as an extensional structure by 3.7 ± 0.2 Ma.

A Pliocene onset of syn-extensional magmatism—an inferred inception of extensional slip on the Mai'iu Fault—appears to be supported by the detrital zircons from the Mai'iu and Bonua Rivers. Because of the dense rainforest cover and inaccessibility of large parts of the footwall of the SDMCC it is unknown whether the samples collected by us from the Paleocene Yau Igneous Complex (~60-57 Ma) and the Plio-Pleistocene granitoids (~3.7-2.0 Ma) cover the full intrusive history of this MCC. Remarkably, although we analyzed in total about 500 zircons from the Mai'iu and Bonua Rivers, modern sediments from these streams draining Mt. Suckling are dominated by zircon $^{206}Pb/^{238}U$ dates between 4 and 2 Ma (Figs. 12a and b). This range is essentially identical to that defined by the lower-intercept ages (~3.7 to ~2.0 Ma) of the Suckling Granite, Mai'iu Monzonite and Bonua Porphyry. Based on these results we infer that syn-extensional magmatism had started by ~4 Ma which is consistent with the oldest known syn-extensional granitoid (~3.7 Ma, PNG-15-61a)

on Mt. Suckling. If any older syn-extensional granitoids exist on Mt. Suckling, we found no evidence for them in samples of detrital zircons from the present-day Mai'iu and Bonua Rivers.

4.4 Further constraints on the Cenozoic history of the SDMCC from detrital zircons

As mentioned above, because of the dense rainforest cover and inaccessibility of large parts of the footwall of the SDMCC it is unknown whether we covered the full intrusive history of this MCC with our samples. Except three concordant Jurassic and Cretaceous $^{206}Pb/^{238}U$ dates in PNG-15-76d, virtually all zircons from the Mai'iu and Bonua Rivers fall within the range of 4-2 Ma, lacking evidence for any other Cenozoic zircon growth. But what happened to the subducted Goropu Metabasalt slab after subduction system suspension and transition to an extensional tectonic regime?

East of Mt. Dayman, Pb_c-corrected zircon $^{206}Pb/^{238}U$ dates reported in an unpublished report (Gordon, 2013) from the Dare Creek and Nauwandowan River draining Mt. Dayman and the Gwoira Conglomerate (5* and 6*; Fig. 3) show a young (or multiple?) subpopulation of dates between ~5 and ~0.1 Ma with a KDE mode at ~3 Ma (Fig. 12c). Zircons from this subpopulation have been described as commonly stubby to rounded with evidence of late to post-magmatic poorly zoned rims (Gordon, 2013). In contrast to our samples from the Mai'iu and Bonua Rivers, those of Gordon (2013) contain a number of younger zircon with $^{206}Pb/^{238}U$ dates between ~1.5 and ~0.1 Ma. No granitoids have been mapped or observed by us in the field

east of Mt. Suckling. Hence, the $^{206}Pb/^{238}U$ dates ranging between ~5 and ~0.1 Ma (Fig. 12c) presented by Gordon (2013) may have a different source.

In contrast to zircons from the rivers draining Mt. Suckling, zircons from those draining Mt. Dayman and the Gwoira Conglomerate contain concordant Permian (~294-286 Ma), Cretaceous (~119-67 Ma) and Paleogene (~61-55 Ma) subpopulations. Based on our zircon U–Pb ages from the Bonenau Schist (~103-72 Ma) and the Yau Igneous Complex (~60-57 Ma), we attribute the Cretaceous and Paleocene-Eocene $^{206}Pb/^{238}U$ dates of the Dare Creek and Nauwandowan River samples (Fig. 12d) to erosion of these units, respectively. As is the case for the Mai'iu and Bonua Rivers that drain Mt. Suckling, no zircon $^{206}Pb/^{238}U$ dates between 55 and 5 Ma have been identified in the study of Gordon (2013). Collectively, the results presented here and those of Gordon (2013) appear to indicate that the Goropu Metabasalt slab was largely unaffected by magmatism throughout the Cenozoic after it had been subducted beneath the CVA in the Paleogene and before extensional reactivation of the Owen Stanley Fault in the Pliocene.

4.5 Evidence about the crustal structure from xenocrystic zircons

Zircon U–Pb analyses in samples of the Suckling Granite, Mai'iu Monzonite, Bonua Porphyry and a basaltic andesite dike yielded zircon $^{206}Pb/^{238}U$ dates that greatly pre-date the youngest subpopulations of the same samples and are inferred to be xenocrysts. These inherited zircons (Fig. 13a) provide constraints on the crustal structure of the SDMCC. Xenocrystic zircon from the syn-extensional

intrusions yielded, amongst younger Cenozoic (~58 to ~15 Ma) and older Jurassic-Mesoproterozoic (~1089 to ~149 Ma) zircons (Table S1)—the former possibly indicating magmatic activity and modifications (associated with tectonic events in the Cenozoic, Fig. S2) of the continental crust that is underlying the basaltic carapace of the SDMCC (see below), and the latter attributed to recycling of older crustal material—$^{206}Pb/^{238}U$ dates between ~106 and ~90 Ma. Similarly, Cretaceous inherited U–Pb ages have been reported from zircons in an 8.1 ± 0.4 Ma-old microgranodiorite (~120-100 Ma; Adshead and Appleby, 1996) on Misima Island and from a 1.98 ± 0.01 Ma-old andesitic dike (~114-90 Ma; DesOrmeau et al., 2014) from Normanby Island (Figs. 1 and 13b). Significantly, this record of Cretaceous xenocrysts in granitoids of the SDMCC compares to $^{206}Pb/^{238}U$ dates on zircon from the Kagi Metamorphics (Kopi et al., 2004) on the northwestern end of the Papuan Peninsula, from the basement gneisses on the D'Entrecasteaux Islands and from the Calvados Schist (DesOrmeau et al., 2014; Zirakparvar et al., 2013) on the Louisiade Archipelago (Figs. 1 and 13c-d). Strikingly, the Cretaceous KDE peaks of each dataset are virtually in phase (Fig. 13), implying a common source.

Our $^{206}Pb/^{238}U$ dates on xenocrystic zircons in the syn-extensional intrusions of the SDMCC match the Aptian-Cenomanian (~125-94 Ma) fossil age assigned to the Kagi Metamorphics (Davies, 2012; Dow et al., 1974; Glaessner, 1949), and we infer that they are sourced from that Australian-plate derived, volcanosedimentary unit. Although the (mapped) surface exposure of the Kagi Metamorphics narrows significantly east of 148°15'E and disappears east of 148°45'E, the occurrence of Cretaceous zircon xenocrysts in the granitoids of the SDMCC implies that they (the Kagi Metamorphics) continue east to underlie basaltic rocks (Goropu Metabasalt)

that form the exposed footwall of this MCC (Fig. 3). Moreover, the above-cited Cretaceous inherited zircon U–Pb ages that continue into the D'Entrecasteaux Islands and Louisiade Archipelago imply that Kagi-equivalent continental crust continues to the north and east of the SDMCC (Fig. 1). This relationship supports the inference of Davies and Smith (1971) who argued that the Mesozoic-aged sialic schists and gneisses form an approximately 900-km long, discontinuous belt along the entire length of the Papuan Peninsula to the islands of the Louisiade Archipelago (Fig. 1)—the continental core of southeastern PNG.

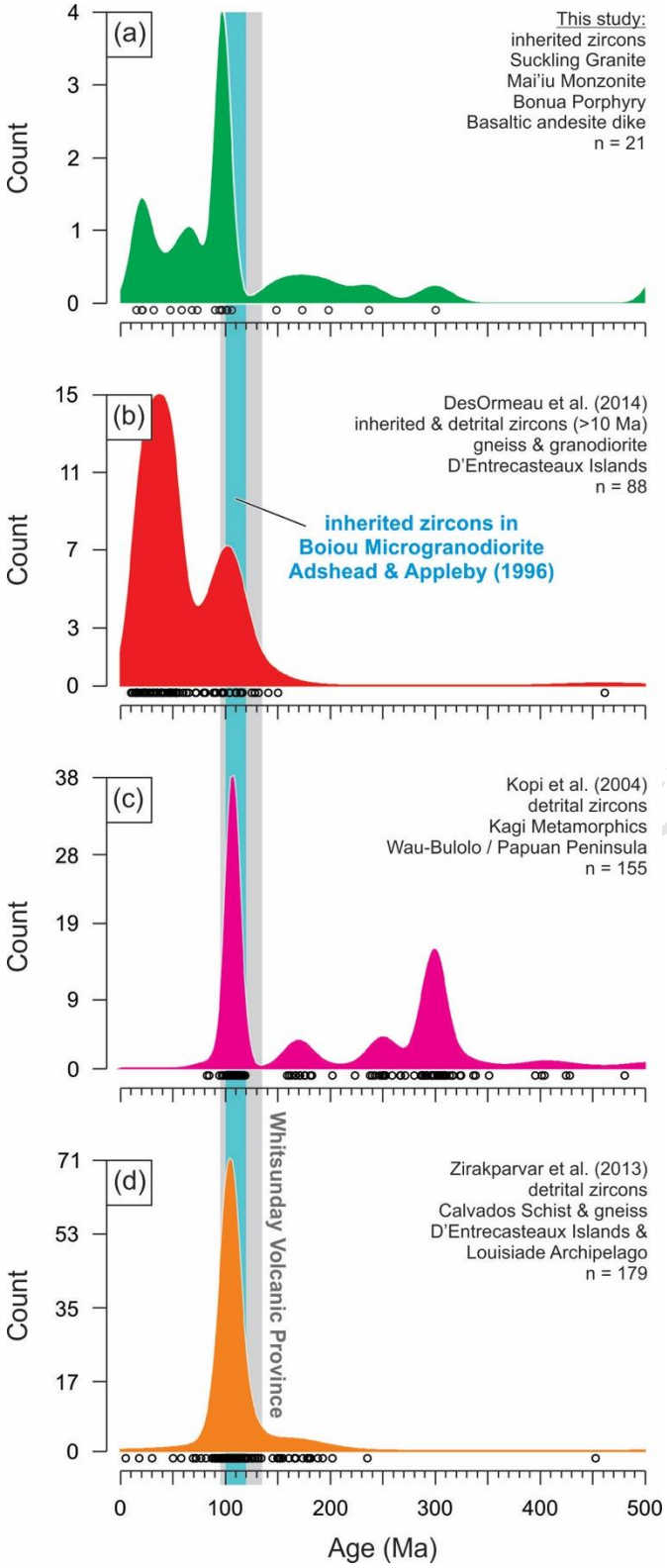

Fig. 13: Kernel density estimation (KDE) diagrams of $^{206}Pb/^{238}U$ dates of inherited zircons from the igneous rocks of the Suckling-Dayman metamorphic core complex (Suckling Granite, Mai'iu Monzonite, Bonua Porphyry, basaltic andesite dike). The

KDE diagram is compared to those from (b) inherited and detrital zircons from Goodenough and Normanby Islands (DesOrmeau et al., 2014), (c) detrital zircons from the Kagi Metamorphics of the northwestern Papuan Peninsula (Kopi et al., 2004) and (d) detrital zircons from Goodenough Island and the Louisiade Archipelago (Zirakparvar et al., 2013). Not shown are detrital zircon U–Pb ages from the Kagi Metamorphics reported by Bodorkos et al. (2013), also from the northwestern Papuan Peninsula, that indicate a Permian maximum depositional age and resemble zircon U–Pb ages from the basement rocks in the eastern Highlands (Van Wyck and Williams, 2002) and the Coen Inlier in northern Queensland (Blewett and Black, 1998; and references therein). The blue bar denotes the age range of inherited zircons from the Boiou Microgranodiorite on Misima Island (Figs. S1 and S2) as reported by Adshead and Appleby (1996). The grey bar marks the duration of igneous activity associated with the Whitsunday Volcanic Province (Bryan et al., 1997; Ewart et al., 1992; Tulloch et al., 2010). Bin and band widths were set to 10 myr.

The zircon U–Pb ages and isotopic composition of this belt of continental crust in southeastern PNG is strikingly similar to Cretaceous-aged volcaniclastic sediments along the coast of Queensland in present-day Australia (Fig. 1a). After Kopi et al. (2004) and Zirakparvar et al. (2013), we infer that the original source region of the detrital zircons in this suite of metasedimentary units (Kagi Metamorphics on the Papuan Peninsula, inherited zircon in the syn-extensional intrusions of the SDMCC, basement gneisses on the D'Entrecasteaux Islands, and Calvados Schist in the Louisiade Archipelago) likely lay on or near what is now the

eastern coast of Australia. The Cretaceous KDE peaks of our dataset and those from the literature (Adshead and Appleby, 1996; DesOrmeau et al., 2014; Kopi et al., 2004; Zirakparvar et al., 2013) are all entirely within the range of Rb–Sr, K–Ar and zircon U–Pb ages (~134-95 Ma, Fig. 13) obtained for rocks in the Whitsunday Volcanic Province (WVP) in eastern Queensland, Australia (Bryan et al., 1997, 2012; Ewart et al., 1992; Tulloch et al., 2010). On the D'Entrecasteaux Islands, ~4.1-1.8 Ma-old intrusions of granodioritic composition yielded essentially the same crystallization ages as the syn-extensional granitoids of the SDMCC (this study; Baldwin and Ireland, 1995; DesOrmeau et al., 2014; Gordon et al., 2012). Recent work on the isotopic composition of deformed granodiorites from Fergusson and Normanby Islands (Korchinski et al., 2014) yielded relatively primitive $^{87}Sr/^{86}Sr_i$ values (0.70380-0.70442) that are similar to those from the WVP (0.70312-0.70440; Ewart et al., 1992), further supporting derivation of these granitoids from WVP-type material.

5. Conclusions

The Suckling-Dayman metamorphic core complex (SDMCC) in the Woodlark Rift in southeastern PNG is being exhumed along an active low-angle normal fault, the Mai'iu Fault. Uplift of this continental metamorphic core complex (MCC) has exposed metasedimentary and metaigneous rocks of Late Cretaceous to Pleistocene age. The dominant footwall unit of the SDMCC, the Goropu Metabasalt, formed in a back-arc basin to the northeast of the Australian continent in the Late Cretaceous possibly between ~103 and ~72 Ma and has a composition transitional

between N and E-MORB. The Goropu Metabasalt was intruded in the Paleocene (between ~60 and ~57 Ma) by gabbroic-tonalitic stocks with MORB affinities (Yau Igneous Complex). Following northward subduction of the Goropu Metabasalt in the Paleogene beneath the Cape Vogel Arc and its basement, the Papuan Ultramafic Belt, the Owen Stanley Fault was inverted as an extensional structure (the Mai'iu Fault). The timing of this inversion is dated by zircon U–Pb crystallization ages of syn-extensional granitoids that have calc-alkaline to high-K compositions. These stocks intruded the footwall of the SDMCC between ~3.7 and ~2.0 Ma and were later decapitated and uplifted as a result of slip on the Mai'iu Fault. The upper end of this range (3.7 ± 0.2 Ma) is inferred to mark the inception of extensional slip on the Mai'iu Fault. This minimum age constraint for the onset of extension on the Mai'iu Fault is supported by detrital zircons in modern streams that predominantly yield U–Pb ages between 4 and 2 Ma. Detrital zircons from streams draining the footwall of the SDMCC indicate that the Goropu Metabasalt slab was largely unaffected by magmatism throughout the Cenozoic after subduction zone suspension and extensional reactivation of the Owen Stanley Fault in the Pliocene. Xenocrystic zircons in the granitoids imply that the crust underlying the metabasaltic carapace of the SDMCC consists of Australian-continent derived Cretaceous sedimentary rocks that are equivalent to those exposed farther northwest in the central Papuan Peninsula as the Kagi Metamorphics.

Acknowledgments

Marsden Grant VUW1310 and NSF Grant EAR-1524729 provided financial support to conduct this research. JEO thanks Lisa Stockli for help with the ICP-MS analyses, Luisa Ashworth for whole-rock trace element analyses and Stacia Gordon for providing additional cathodoluminescence images. We are grateful to Hugh Davies (retired from University of Papua New Guinea) and Ian Smith (University of Auckland) for providing field book scans and discussions, and John Oa (Papua New Guinea National Mapping Bureau) and Jane Black (Doc Fisher Geosciences Library) for copies and access to aerial photos and field sheets. We thank Ian Smith and Nathan Daczko for providing samples. Further thanks go to Nathan Daczko for providing the unpublished report of Kristina Gordon. Special thanks go to the many landowners, oral chiefs, elders and citizens who granted us permission to study their land. We are very grateful for our guides and carriers without whom this work would not have been possible. Comments from Laura Webb and two anonymous helped improve the quality of this manuscript.

The authors declare that there is no conflict of interest.

References

Abers, G.A., Eilon, Z., Gaherty, J.B., Jin, G., Kim, YH., Obrebski, M., Dieck, C., 2016. Southeast Papuan crustal tectonics: Imaging extension and buoyancy of an active rift. J. Geophys. Res. Solid Earth 121, 951–971. https://doi.org/10.1002/2015JB012621

Abers, G.A., Roecker, S.W., 1991. Deep structure of an arc-continent collision: Earthquake relocation and inversion for upper mantle P and S wave velocities beneath Papua New Guinea. J. Geophys. Res. Solid Earth 96, 6379–6401. https://doi.org/10.1029/91JB00145

Adshead, N., Appleby, A.-K., 1996. The Umuna Au-Ag deposit, Misima Island, Papua New Guinea: Spatially but not genetically associated with porphyry. Australian Mineral Foundation, Glenside, Australia.

Arevalo, R., McDonough, W.F., 2010. Chemical variations and regional diversity observed in MORB. Chem. Geol. 271, 70–85. https://doi.org/10.1016/j.chemgeo.2009.12.013

Baker, G., 1946. Preliminary note on volcanic eruptions in the Goropu Mountains, Southeastern Papua, during the period December, 1943, to August, 1944. J. Geol. 54, 19–31. https://doi.org/10.1086/625315

Baldwin, S.L., Fitzgerald, P.G., Webb, L.E., 2012. Tectonics of the New Guinea Region. Annu. Rev. Earth Planet. Sci. 40, 495–520. https://doi.org/10.1146/annurev-earth-040809-152540

Baldwin, S.L., Ireland, T.R., 1995. A tale of two eras: Pliocene-Pleistocene unroofing of Cenozoic and late Archean zircons from active metamorphic core complexes, Solomon Sea, Papua New Guinea. Geology 23, 1023–1026.

Baldwin, S.L., Monteleone, B.D., Webb, L.E., Fitzgerald, P.G., Grove, M., Hill, J.E., 2004. Pliocene eclogite exhumation at plate tectonic rates in eastern Papua New Guinea. Nature 431, 263–267.

Baldwin, S.L., Webb, L.E., Monteleone, B.D., 2008. Late Miocene coesite-eclogite exhumed in the Woodlark Rift. Geology 36, 735–738.

Belford, D.J., 1976. Foraminifera and age of samples from southeastern Papua (No. 1976/165). Bureau of Mineral Resources, Geology and Geophysics, Canberra, Australia.

Blewett, R.S., Black, L.P., 1998. Structural and temporal framework of the Coen Region, north Queensland: Implications for major tectonothermal events in east and north Australia. Aust. J. Earth Sci. 45, 597–609. https://doi.org/10.1080/08120099808728415

Bodorkos, S., Sheppard, S., Saroa, D., Tsiperau, C.U., Sircombe, K.N., 2013. New SHRIMP U–Pb zircon ages from the Wau-Bulolo region, Papua New Guinea, Mineral Resources Authority of Papua New Guinea Technical Note, TN 2013/05. Geoscience Australia.

Brown, C.M., 1977. Yule - Papua New Guinea, Sheet SC/55-2 International Index. Geological Series - Explanatory Notes.

Bryan, S.E., Constantine, A.E., Stephens, C.J., Ewart, A., Schön, R.W., Parianos, J., 1997. Early Cretaceous volcano-sedimentary successions along the eastern Australian continental margin: Implications for the break-up of eastern Gondwana. Earth Planet. Sci. Lett. 153, 85–102. https://doi.org/10.1016/S0012-821X(97)00124-6

Bryan, S.E., Cook, A., Allen, C.M., Siégel, C., Purdy, D., Greentree, J., Uysal, T., 2012. Early-mid Cretaceous tectonic evolution of eastern Gondwana: from silicic LIP magmatism to continental rupture. Episodes 35, 142–152.

Bulois, C., Pubellier, M., Chamot-Rooke, N., Delescluse, M., 2017. Successive Rifting Events in Marginal Basins: The Example of the Coral Sea Region (Papua New Guinea). Tectonics 37, 3–29. https://doi.org/10.1002/2017TC004783

Caffi, P., 2008. Evolution of an active metamorphic core complex, Suckling-Dayman Massif, eastern Papua New Guinea (BSc Honor's thesis). Macquarie University, Sydney, Australia.

Cameron, M.L., 2014. Rifting and subduction in the Papuan Peninsula, Papua New Guinea: The significance of the Trobriand Trough, the Nubara strike-slip fault, and the Woodlark Rift to the present configuration of Papua New Guinea (PhD thesis). The University of Alabama, Tuscaloosa, Alabama.

Catalano, J.P., 2012. Geochemical and $^{40}Ar/^{39}Ar$ constraints on the evolution of volcanism in the Woodlark Rift, Papua New Guinea (MSc Thesis). Syracuse University.

Chappell, B.W., White, A.J.R., 1974. Two contrasting granite types. Pac. Geol. 8, 173–174.

Cloos, M., Sapiie, B., Quarles van Ufford, A., Weiland, R.J., Warren, P.Q., McMahon, T.P., 2005. Collisional delamination in New Guinea: The geotectonics of subducting slab breakoff, in: Cloos, M., Sapiie, B., Quarles van Ufford, A., Weiland, R.J., Warren, P. Q., McMahon, T.P. (Eds.), Collisional Delamination in New Guinea: The Geotectonics of Subducting Slab Breakoff, Geological Society of America Special Paper. Geological Society of America, pp. 1–51.

Cluzel, D., Aitchison, J.C., Picard, C., 2001. Tectonic accretion and underplating of mafic terranes in the Late Eocene intraoceanic fore-arc of New Caledonia (Southwest Pacific): geodynamic implications. Tectonophysics 340, 23–59. https://doi.org/10.1016/S0040-1951(01)00148-2

Cooper, P., Taylor, B., 1987. Seismotectonics of New Guinea: A model for arc reversal following arc-continent collision. Tectonics 6, 53–67. https://doi.org/10.1029/TC006i001p00053

Corfu, F., Hanchar, J.M., Hoskin, P.W.O., Kinny, P., 2003. Atlas of Zircon Textures. Rev. Mineral. Geochem. 53, 469–500. https://doi.org/10.2113/0530469

Daczko, N.R., Caffi, P., Halpin, J.A., Mann, P., 2009. Exhumation of the Dayman dome metamorphic core complex, eastern Papua New Guinea. J. Metamorph. Geol. 27, 405–422. https://doi.org/10.1111/j.1525-1314.2009.00825.x

Daczko, N.R., Caffi, P., Mann, P., 2011. Structural evolution of the Dayman dome metamorphic core complex, eastern Papua New Guinea. GSA Bull. 123, 2335–2351. https://doi.org/10.1130/B30326.1

D'Addario, G.W., Dow, D.B., Swoboda, R., 1976. Geology of Papua New Guinea.

Davies, H.L., 2012. The geology of New Guinea—the cordilleran margin of the Australian continent. Episodes 35, 87–102.

Davies, H.L., 1980. Folded thrust fault and associated metamorphism in the Suckling-Dayman massif, Papua New Guinea. Am. J. Sci. 280-A, 171–191.

Davies, H.L., Jaques, A.L., 1984. Emplacement of ophiolite in Papua New Guinea. Geol. Soc. Lond. Spec. Publ. 13, 341–349. https://doi.org/10.1144/GSL.SP.1984.013.01.27

Davies, H.L., Perembo, R.C.B., Winn, R.D., KenGemar, P., 1997. Terranes of the New Guinea Orogen, in: Hancock, G. (Ed.), Proceedings of the PNG Geology, Exploration and Mining Conference. Australasian Institute of Mining and Metallurgy, Madang, Papua New Guinea, pp. 61–66.

Davies, H.L., Smith, I.E.M., 1974. Tufi-Cape Nelson - Papua New Guinea, Sheet SC/55-8,4 International Series. Geological Series - Explanatory Notes.

Davies, H.L., Smith, I.E.M., 1971. Geology of Eastern Papua. GSA Bull. 82, 3299–3312.

Davies, H.L., Symonds, P.A., Ripper, I.D., 1984. Structure and evolution of the southern Solomon Sea region. BMR J. Aust. Geol. Geophys. 9, 49–68.

Davies, H.L., Warren, R.G., 1988. Origin of eclogite-bearing, domed, layered metamorphic complexes ("core complexes") in the D'Entrecasteaux Islands, Papua New Guinea. Tectonics 7, 1–21. https://doi.org/10.1029/TC007i001p00001

DesOrmeau, J.W., Gordon, S.M., Little, T.A., Bowring, S.A., 2014. Tracking the exhumation of a Pliocene (U)HP terrane: U-Pb and trace-element constraints from zircon, D'Entrecasteaux Islands, Papua New Guinea. Geochem. Geophys. Geosystems 15, 3945–3964. https://doi.org/10.1002/2014GC005396

Dow, D.B., 1977. A geological synthesis of Papua New Guinea. Bur Min. Resour Aust Bull 201, 1–41.

Dow, D.B., Smit, J.A.J., Bain, J.H.C., Ryburn, R.J., 1972. Geology of the South Sepik Region, New Guinea (No. 1972/133), Bulletin. Bureau of Mineral Resources, Geology and Geophysics, Canberra, Australia.

Dow, D.B., Smit, J.A.J., Page, R.W., 1974. Wau - Papua New Guinea, Sheet SB/55-14 International Index. Geological Series - Explanatory Notes.

Drummond, B.J., Collins, C.D.N., Gibson, G., 1979. The crustal structure of the Gulf of Papua and northwest Coral Sea. BMR J. Aust. Geol. Geophys. 4, 341–351.

Eilon, Z., Abers, G.A., Gaherty, J., Jin, G., 2015. Imaging continental breakup using teleseismic body waves: The Woodlark Rift, Papua New Guinea. Geochem. Geophys. Geosystems 16, 2529–2548. https://doi.org/10.1002/2015GC005835

Eissen, J.-P., Crawford, A.J., Cotten, J., Meffre, S., Bellon, H., Delaune, M., 1998. Geochemistry and tectonic significance of basalts in the Poya Terrane, New Caledonia. Tectonophysics 284, 203–219. https://doi.org/10.1016/S0040-1951(97)00183-2

Ewart, A., Schon, R.W., Chappell, B.W., 1992. The Cretaceous volcanic-plutonic province of the central Queensland (Australia) coast—a rift related 'calc-alkaline' province. Earth Environ. Sci. Trans. R. Soc. Edinb. 83, 327–345. https://doi.org/10.1017/S0263593300008002

Falvey, D.A., Pritchard, T., 1982. Preliminary palaeomagnetic results from northern Papua New Guinea: evidence for large microplate rotations, in: Transactions Third Circum-Pacific Energy and Mineral Resources Conference. Hawaii, pp. 593–599.

Ferris, A., Abers, G.A., Zelt, B., Taylor, B., Roecker, S., 2006. Crustal structure across the transition from rifting to spreading: the Woodlark rift system of Papua New Guinea. Geophys. J. Int. 166, 622–634. https://doi.org/10.1111/j.1365-246X.2006.02970.x

Francis, G., Lock, J., Okuda, Y., 1987. Seismic stratigraphy and structure of the area to the southeast of the trobriand platform. Geo-Mar. Lett. 7, 121–128. https://doi.org/10.1007/BF02238041

Gaina, C., Müller, D., 2007. Cenozoic tectonic and depth/age evolution of the Indonesian gateway and associated back-arc basins. Earth-Sci. Rev. 83, 177–203. https://doi.org/10.1016/j.earscirev.2007.04.004

Gaina, C., Müller, D.R., Royer, J., Symonds, P., 1999. Evolution of the Louisiade triple junction. J. Geophys. Res. Solid Earth 104, 12927–12939. https://doi.org/10.1029/1999JB900038

Geological Survey of Papua New Guinea, British Geological Survey, 2004. Gravity map of Papua New Guinea.

Gill, J.B., Morris, J.D., Johnson, R.W., 1993. Timescale for producing the geochemical signature of island arc magmas: U-Th-Po and Be-B systematics in recent Papua New Guinea lavas. Geochim. Cosmochim. Acta 57, 4269–4283. https://doi.org/10.1016/0016-7037(93)90322-N

Glaessner, M.F., 1949. Mesozoic fossils from the Snake River, Central New Guinea. Qld. Mus Mem 12, 165–180.

Glen, R.A., Meffre, S., 2009. Styles of Cenozoic collisions in the western and southwestern Pacific and their applications to Palaeozoic collisions in the Tasmanides of eastern Australia. Tectonophysics, Arc-continent Collision 479, 130–149. https://doi.org/10.1016/j.tecto.2009.03.023

Gordon, K., 2013. Detrital zircon provenance study, Mount Dayman, Papua New Guinea (Coursework for partial completion of Honours in Geology). Macquarie University, Sydney, Australia.

Gordon, S.M., Little, T.A., Hacker, B.R., Bowring, S.A., Korchinski, M., Baldwin, S.L., Kylander-Clark, A.R.C., 2012. Multi-stage exhumation of young UHP–HP rocks: Timescales of melt crystallization in the D'Entrecasteaux Islands, southeastern Papua New Guinea. Earth Planet. Sci. Lett. 351–352, 237–246. https://doi.org/10.1016/j.epsl.2012.07.014

Hall, R., 2002. Cenozoic geological and plate tectonic evolution of SE Asia and the SW Pacific: computer-based reconstructions, model and animations. Journal of Asian Earth Sciences, 20, 353–431. https://doi.org/10.1016/S1367-9120(01)00069-4

Hastie, A.R., Kerr, A.C., Pearce, J.A., Mitchell, S.F., 2007. Classification of altered volcanic island arc rocks using immobile trace elements: development of the Th–Co discrimination diagram. J. Petrol. 48, 2341–2357. https://doi.org/10.1093/petrology/egm062

Hiess, J., Condon, D.J., McLean, N., Noble, S.R., 2012. $^{238}U/^{235}U$ systematics in terrestrial uranium-bearing minerals. Science 335, 1610–1614. https://doi.org/10.1126/science.1215507

Hill, K.C., Gleadow, A.J.W., 1990. Apatite fission track analysis of the Papuan Basin, in: Carman, G.J., Carman, Z. (Eds.), Petroleum Exploration and Development in Papua New

Guinea: Proceedings of the First PNG Petroleum Convention. Port Moresby, Papua New Guinea, pp. 119–136.

Hill, K.C., Hall, R., 2003. Mesozoic–Cenozoic evolution of Australia's New Guinea margin in a west Pacific context., in: Hillis, R.R., Müller, R.D. (Eds.), Evolution and Dynamics of the Australian Plate, Geological Society of Australia Special Publication. pp. 265–290.

Holm, R.J., Poke, B., 2018. Petrology and crustal inheritance of the Cloudy Bay Volcanics as derived from a fluvial conglomerate, Papuan Peninsula (Papua New Guinea): An example of geological inquiry in the absence of in situ outcrop. Cogent Geosci. 4, 1450198. https://doi.org/10.1080/23312041.2018.1450198

Holm, R.J., Rosenbaum, G., Richards, S.W., 2016. Post 8 Ma reconstruction of Papua New Guinea and Solomon Islands: Microplate tectonics in a convergent plate boundary setting. Earth-Sci. Rev. 156, 66–81. https://doi.org/10.1016/j.earscirev.2016.03.005

Holm, R.J., Spandler, C., Richards, S.W., 2015. Continental collision, orogenesis and arc magmatism of the Miocene Maramuni arc, Papua New Guinea. Gondwana Res. 28, 1117–1136. https://doi.org/10.1016/j.gr.2014.09.011

Holm, R.J., Spandler, C., Richards, S.W., 2013. Melanesian arc far-field response to collision of the Ontong Java Plateau: Geochronology and petrogenesis of the Simuku Igneous Complex, New Britain, Papua New Guinea. Tectonophysics 603, 189–212. https://doi.org/10.1016/j.tecto.2013.05.029

Holm, R.J., Tapster, S., Jelsma, H.A., Rosenbaum, G., Mark, D.F., 2019. Tectonic evolution and copper-gold metallogenesis of the Papua New Guinea and Solomon Islands region. Ore Geol. Rev. 104, 208–226. https://doi.org/10.1016/j.oregeorev.2018.11.007

Horstwood, M.S.A., Košler, J., Gehrels, G., Jackson, S.E., McLean, N.M., Paton, C., Pearson, N.J., Sircombe, K., Sylvester, P., Vermeesch, P., Bowring, J.F., Condon, D.J., Schoene, B., 2016. Community-derived standards for LA-ICP-MS U-(Th-)Pb geochronology – uncertainty propagation, age interpretation and data reporting. Geostand. Geoanalytical Res. 40, 311–332. https://doi.org/10.1111/j.1751-908X.2016.00379.x

Hu, Z., Zhang, W., Liu, Y., Chen, H., Gaschnig, R.M., Zong, K., Li, M., Gao, S., Hu, S., 2013. Rapid bulk rock decomposition by ammonium fluoride (NH4F) in open vessels at an elevated digestion temperature. Chem. Geol. 355, 144–152. https://doi.org/10.1016/j.chemgeo.2013.06.024

Ito, H., Spencer, C.J., Danišík, M., Hoiland, C.W., 2017. Magmatic tempo of Earth's youngest exposed plutons as revealed by detrital zircon U–Pb geochronology. Sci. Rep. 7, 12457. https://doi.org/10.1038/s41598-017-12790-w

Jackson, S.E., Pearson, N.J., Griffin, W.L., Belousova, E.A., 2004. The application of laser ablation-inductively coupled plasma-mass spectrometry to in situ U–Pb zircon geochronology. Chem. Geol. 211, 47–69. https://doi.org/10.1016/j.chemgeo.2004.06.017

Jaques, A.L., Chappell, B.W., 1980. Petrology and trace element geochemistry of the Papuan Ultramafic Belt. Contrib. Mineral. Petrol. 75, 55–70. https://doi.org/10.1007/BF00371889

Jin, G., Gaherty, J.B., Abers, G.A., Kim, Y., Eilon, Z., Buck, R.W., 2015. Crust and upper mantle structure associated with extension in the Woodlark Rift, Papua New Guinea from Rayleigh-

wave tomography. Geochem. Geophys. Geosystems 16, 3808–3824. https://doi.org/10.1002/2015GC005840

Johnson, R.W., Mackenzie, D.E., Smith, I.E.M., 1978. Delayed partial melting of subduction-modified mantle in Papua New Guinea. Tectonophysics 46, 197–216. https://doi.org/10.1016/0040-1951(78)90114-2

Joshima, M., Honza, E., 1986. Age estimation of the Solomon Sea based on heat flow data. Geo-Marine Letters 6, 211–217. https://doi.org/10.1007/BF02239582

Joshima, M., Okuda, Y., Murakami, F., Kishimoto, K., Honza, E., 1986. Age of the Solomon Sea Basin from magnetic lineations. Geo-Marine Letters 6, 229–234. https://doi.org/10.1007/BF02239584

Knesel, K.M., Cohen, B.E., Vasconcelos, P.M., Thiede, D.S., 2008. Rapid change in drift of the Australian plate records collision with Ontong Java plateau. Nature 454, 754.

Kopi, G., Findlay, R.H., Williams, I., 2004. Age and provenance of the Owen Stanley Metamorphic Complex, East Papuan Composite Terrane, Papua New Guinea. Geological Survey of Papua New Guinea (unpublished report), Port Moresby, Papua New Guinea.

Korchinski, M.S., Vry, J., Little, T.A., Millet, M.-A., Bicknell, R., Smith, E., Handt, A., 2014. Timing of UHP exhumation and rock fabric development in gneiss domes containing the world's youngest eclogite Facies rocks, southeastern Papua New Guinea. J. Metamorph. Geol. 32, 1019–1039. https://doi.org/10.1111/jmg.12105

Koulali, A., Tregoning, P., McClusky, S., Stanaway, R., Wallace, L., Lister, G., 2015. New Insights into the present-day kinematics of the central and western Papua New Guinea from GPS. Geophysical Journal International 202, 993–1004. https://doi.org/10.1093/gji/ggv200

Lancaster, P.J., Strachan, R.A., Bullen, D., Fowler, M., Jaramillo, M., Saldarriaga, A.M., 2017. U–Pb zircon geochronology and geodynamic significance of 'Newer Granite' plutons in Shetland, northernmost Scottish Caledonides. J. Geol. Soc. 174, 486–497. https://doi.org/10.1144/jgs2016-106

Latter, J.H., 1964. Explanatory notes to accompany a geological sketch map of part of the Western Daga Ranges, Papua (No. 113). Bureau of Mineral Resources, Geology and Geophysics, Canberra, Australia.

Le Maitre, R.W., Streckeisen, A., Zanettin, B., Le Bas, M.J., Bonin, B., Bateman, P. (Eds.), 2002. Igneous Rocks: A Classification and Glossary of Terms: Recommendations of the International Union of Geological Sciences Subcommission on the Systematics of Igneous Rocks, 2nd ed. Cambridge University Press, Cambridge. https://doi.org/10.1017/CBO9780511535581

Lindley, I.D., 2014. Suckling Dome and the Australian–Woodlark plate boundary in eastern Papua: the geology of the Keveri and Ada'u Valleys. Aust. J. Earth Sci. 61, 1125–1147. https://doi.org/10.1080/08120099.2014.965980

Lissenberg, C.J., Rioux, M., Shimizu, N., Bowring, S.A., Mével, C., 2009. Zircon Dating of Oceanic Crustal Accretion. Science 323, 1048–1050. https://doi.org/10.1126/science.1167330

Little, T.A., Baldwin, S.L., Fitzgerald, P.G., Monteleone, B.D., 2007. Continental rifting and metamorphic core complex formation ahead of the Woodlark spreading ridge,

D'Entrecasteaux Islands, Papua New Guinea. Tectonics 26, 1–26. https://doi.org/10.1029/2005TC001911

Little, T.A., Webber, S., Mizera, M., Boulton, C., Oesterle, J., Ellis, S., Boles, A., van der Pluijm, B., Norton, K., Seward, D., Biemiller, J., Wallace, L.M., 2019. Evolution of a rapidly slipping, active low-angle normal fault, Suckling-Dayman Metamorphic Core Complex, SE Papua New Guinea. GSA Bull. https://doi.org/10.1130/B35051.1

Lus, W.Y., McDougall, I., Davies, H.L., 2004. Age of the metamorphic sole of the Papuan Ultramafic Belt ophiolite, Papua New Guinea. Tectonophysics 392, 85–101. https://doi.org/10.1016/j.tecto.2004.04.009

Macnab, R.P., 1969. Geology of the Aroa - upper Dilava - Auga - Middle Angabunga Rivers area, Papua (No. 69/126). Bureau of Mineral Resources, Geology and Geophysics, Canberra, Australia.

Marsh, J.H., Stockli, D.F., 2015. Zircon U–Pb and trace element zoning characteristics in an anatectic granulite domain: Insights from LASS-ICP-MS depth profiling. Lithos 239, 170–185. https://doi.org/10.1016/j.lithos.2015.10.017

McDougall, I., Harrison, T.M., 1999. Geochronology and Thermochronology by the $^{40}Ar/^{39}Ar$ method. Oxford University Press, New York, USA.

Miller, J.S., Matzel, J.E.P., Miller, C.F., Burgess, S.D., Miller, R.B., 2007. Zircon growth and recycling during the assembly of large, composite arc plutons. J. Volcanol. Geotherm. Res., Large Silicic Magma Systems 167, 282–299. https://doi.org/10.1016/j.jvolgeores.2007.04.019

Milsom, J., 1973. The gravity field of the Papuan Peninsula. Geol. En Mijnb. 52, 13–20.

Morrison, G.W., 1980. Characteristics and tectonic setting of the shoshonite rock association. Lithos 13, 97–108. https://doi.org/10.1016/0024-4937(80)90067-5

Nion, S.T.S., Rogerson, R., Griffin, T.J., Arnold, G.O., 1987. Introduction to the geology of the Uyaknji Complex, Papua New Guinea (No. 87/20). Geological Survey of Papua New Guinea.

Ott, B., Mann, P., 2015. Late Miocene to Recent formation of the Aure-Moresby fold-thrust belt and foreland basin as a consequence of Woodlark microplate rotation, Papua New Guinea. Geochem. Geophys. Geosystems 16, 1988–2004. https://doi.org/10.1002/2014GC005668

Page, R.W., 1976. Geochronology of igneous and metamorphic rocks in the New Guinea Highlands. Bull Aust Bur Miner. Resour 162, 125.

Paton, C., Hellstrom, J., Paul, B., Woodhead, J., Hergt, J., 2011. Iolite: Freeware for the visualisation and processing of mass spectrometric data. J Anal Spectrom 26, 2508–2518. https://doi.org/10.1039/C1JA10172B

Pearce, J.A., 2008. Geochemical fingerprinting of oceanic basalts with applications to ophiolite classification and the search for Archean oceanic crust. Lithos, Links Between Ophiolites and LIPs in Earth History 100, 14–48. https://doi.org/10.1016/j.lithos.2007.06.016

Pearce, J.A., Harris, N.B.W., Tindle, A.G., 1984. Trace element discrimination diagrams for the tectonic interpretation of granitic rocks. J. Petrol. 25, 956–983. https://doi.org/10.1093/petrology/25.4.956

Pearce, J.A., Parkinson, I.J., 1993. Trace element models for mantle melting: application to volcanic arc petrogenesis. Geol. Soc. Lond. Spec. Publ. 76, 373. https://doi.org/10.1144/GSL.SP.1993.076.01.19

Peccerillo, A., Taylor, S.R., 1976. Geochemistry of eocene calc-alkaline volcanic rocks from the Kastamonu area, Northern Turkey. Contrib. Mineral. Petrol. 58, 63–81. https://doi.org/10.1007/BF00384745

Peters, K.J., 2007. Tectonic evolution of a metamorphic core complex on Misima Island and implications for the history of continental extension in the Woodlark Rift, southeastern Papua New Guinea (Master of Science). Victoria University of Wellington, Wellington, New Zealand.

Petersen, K.D., Buck, R.W., 2015. Eduction, extension, and exhumation of ultrahigh-pressure rocks in metamorphic core complexes due to subduction initiation. Geochem. Geophys. Geosystems 16, 2564–2581. https://doi.org/10.1002/2015GC005847

Petrus, J.A., Kamber, B.S., 2012. VizualAge: A novel approach to laser ablation ICP-MS U–Pb geochronology data reduction. Geostand. Geoanalytical Res. 36, 247–270. https://doi.org/10.1111/j.1751-908X.2012.00158.x

Pieters, P.E., 1978. Port Moresby-Kalo-Aroa - Papua New Guinea, Sheets SC/55-6, 7 and 11 International Index. Geological Series - Explanatory Notes.

Rioux, M., Johan Lissenberg, C., McLean, N.M., Bowring, S.A., MacLeod, C.J., Hellebrand, E., Shimizu, N., 2012. Protracted timescales of lower crustal growth at the fast-spreading East Pacific Rise. Nat. Geosci. 5, 275–278.

Rogerson, R., Williamson, A., Francis, G., 1986. Recent advances in the knowledge of geology, energy resources and metallogenesis of Papua New Guinea since 1981, in: GEOSEA V Proceedings Vol . II, Geol. Soc. Malaysia Bulletin. pp. 23–37.

Rogerson, R.J., Hilyard, D.B., 1989. Scrapland: A suspect composite Terrane in Papua New Guinea (No. 1989/11). Geological Survey of Papua New Guinea.

Rogerson, R.J., Queen, L., Joseph, L., Lloyd, A., Webb, A., Booth, G., 1991. New stratigraphic and whole-rock geochemical data from the Waria river area, northern Papuan Peninsula (No. 1991/7). Geological Survey of Papua New Guinea.

Rubatto, D., Gebauer, D., Fanning, M., 1998. Jurassic formation and Eocene subduction of the Zermatt–Saas-Fee ophiolites: implications for the geodynamic evolution of the Central and Western Alps. Contrib. Mineral. Petrol. 132, 269–287. https://doi.org/10.1007/s004100050421

Ruprecht, P., Plank, T.A., Jin, G., Abers, G.A., 2013. Rifting and UHP exhumation in Eastern Papua New Guinea: Temperature and pressure constraints from primitive magmas. Presented at the AGU Fall Meeting 2013, San Francisco, USA.

Ruxton, B.P., 1966. Correlation and stratigraphy of dacitic ash-fall layers in northeastern Papua. J. Geol. Soc. Aust. 13, 41–67. https://doi.org/10.1080/00167616608728605

Sano, Y., Tsutsumi, Y., Terada, K., Kaneoka, I., 2002. Ion microprobe U–Pb dating of Quaternary zircon: implication for magma cooling and residence time. J. Volcanol. Geotherm. Res. 117, 285–296. https://doi.org/10.1016/S0377-0273(02)00297-4

Schaltegger, U., Davies, J.H.F.L., 2017. Petrochronology of zircon and baddeleyite in igneous rocks: Reconstructing magmatic processes at aigh temporal resolution. Rev. Mineral. Geochem. 83, 297–328. https://doi.org/10.2138/rmg.2017.83.10

Schärer, U., 1984. The effect of initial ^{230}Th disequilibrium on young U–Pb ages: the Makalu case, Himalaya. Earth Planet. Sci. Lett. 67, 191–204. https://doi.org/10.1016/0012-821X(84)90114-6

Seton, M., Mortimer, N., Williams, S., Quilty, P., Gans, P., Meffre, S., Micklethwaite, S., Zahirovic, S., Moore, J., Matthews, K.J., 2016. Melanesian back-arc basin and arc development: Constraints from the eastern Coral Sea. Gondwana Res. 39, 77–95. https://doi.org/10.1016/j.gr.2016.06.011

Shand, S.J., 1947. The eruptive rocks, 3rd ed. John Wiley & Sons, New York, USA.

Siivola, J., Schmid, R., 2007. Recommendations by the IUGS Subcommission on the Systematics of Metamorphic Rocks: List of mineral abbreviations. Web version 01.02.07. [WWW Document]. IUGS Comm. Syst. Petrol. URL http://www.bgs.ac.uk/scmr/docs/papers/paper_12.pdf

Sláma, J., Košler, J., Condon, D.J., Crowley, J.L., Gerdes, A., Hanchar, J.M., Horstwood, M.S.A., Morris, G.A., Nasdala, L., Norberg, N., Schaltegger, U., Schoene, B., Tubrett, M.N., Whitehouse, M.J., 2008. Plešovice zircon — A new natural reference material for U–Pb and Hf isotopic microanalysis. Chem. Geol. 249, 1–35. https://doi.org/10.1016/j.chemgeo.2007.11.005

Smith, I.E.M., 2013. The chemical characterization and tectonic significance of ophiolite terrains in southeastern Papua New Guinea. Tectonics 32, 159–170. https://doi.org/10.1002/tect.20023

Smith, I.E.M., 1976. Peralkaline rhyolites from the D'Entrecasteaux Islands, Papua New Guinea, in: Johnson, R.W. (Ed.), Volcanism in Australasia. Elsevier, Amsterdam, pp. 275–286.

Smith, I.E.M., 1972. High-potassium intrusives from southeastern Papua. Contrib. Mineral. Petrol. 34, 167–176. https://doi.org/10.1007/BF00373771

Smith, I.E.M., Chappell, B.W., Ward, G.K., Freeman, R.S., 1977. Peralkaline rhyolites associated with andesitic arcs of the southwest Pacific. Earth Planet. Sci. Lett. 37, 230–236. https://doi.org/10.1016/0012-821X(77)90167-4

Smith, I.E.M., Davies, H.L., 1976. Geology of the southeast Papuan mainland (No. 1976/165). Bureau Miner. Resour. J. Aust. Geol. Geophys.

Smith, I.E.M., Davies, H.L., 1973a. Abau - Papua New Guinea, Sheet SC/55-12 International Index. Geological Series - Explanatory Notes.

Smith, I.E.M., Davies, H.L., 1973b. Samarai - Papua New Guinea, Sheet SC/56-9 International Index. Geological Series - Explanatory Notes.

Stacey, J.S., Kramers, J.D., 1975. Approximation of terrestrial lead isotope evolution by a two-stage model. Earth Planet. Sci. Lett. 26, 207–221. https://doi.org/10.1016/0012-821X(75)90088-6

Steiger, R.H., Jaeger, E., 1977. Subcommission of geochronology: convention on the use of decay constants in geo-and cosmochronology. Earth Planet. Sci. Lett. 36, 359–362. https://doi.org/doi:10.1016/0012-821X(77)90060-7

Tapster, S., Roberts, N.M.W., Petterson, M.G., Saunders, A.D., Naden, J., 2014. From continent to intra-oceanic arc: Zircon xenocrysts record the crustal evolution of the Solomon island arc. Geology 42, 1087–1090. https://doi.org/10.1130/G36033.1

Taylor, B., Goodliffe, A.M., Martinez, F., 1999. How continents break up: Insights from Papua New Guinea. J. Geophys. Res. Solid Earth 104, 7497–7512. https://doi.org/10.1029/1998JB900115

Taylor, B., Huchon, P., 2002. Active continental extension in the western Woodlark Basin: A synthesis of Leg 180 results, in: Huchon, P., Taylor, B., Klaus, A. (Eds.), Proceedings of the Ocean Drilling Program, Scientific Results. pp. 1–36.

Tregoning, P., Lambeck, K., Stolz, A., Morgan, P., McClusky, S.C., Beek, P., McQueen, H., Jackson, R.J., Little, R.P., Laing, A., Murphy, B., 1998. Estimation of current plate motions in Papua New Guinea from Global Positioning System observations. Journal of Geophysical Research: Solid Earth 103, 12181–12203. https://doi.org/10.1029/97JB03676

Tulloch, A., Ramezan, J., Faure, K., Allibone, A., 2010. Early Cretaceous magmatism in New Zealand and Queensland: intra-plate or intra-arc origin?, in: Buckman, S., Blevin, P.L. (Eds.), New England Orogen 2010 Conference Proceedings. University of New England, Armidale, pp. 332–335.

van Ufford, A.Q., Cloos, M., 2005. Cenozoic tectonics of New Guinea. AAPG Bull. 89, 119–140. https://doi.org/10.1306/08300403073

Van Wyck, N., Williams, I.S., 2002. Age and provenance of basement metasediments from the Kubor and Bena Bena Blocks, central Highlands, Papua New Guinea: constraints on the tectonic evolution of the northern Australian cratonic margin. Aust. J. Earth Sci. 49, 565–577. https://doi.org/10.1046/j.1440-0952.2002.00938.x

Vermeesch, P., 2018. IsoplotR: A free and open toolbox for geochronology. Geosci. Front. 9, 1479–1493. https://doi.org/10.1016/j.gsf.2018.04.001

Wai, K.M., Abbott, M.J., Grady, A.E., 1994. The Sadowa Igneous Complex, Eastern Papua New Guinea: Ophiolite or not?, in: Goldschmidt Conference. Edinburgh, pp. 949–950.

Walker, D.A., McDougall, I., 1982. $^{40}Ar/^{39}Ar$ and K–Ar dating of altered glassy volcanic rocks: the Dabi Volcanics, P.N.G. Geochim. Cosmochim. Acta 46, 2181–2190. https://doi.org/10.1016/0016-7037(82)90193-4

Wallace, L.M., Ellis, S., Little, T., Tregoning, P., Palmer, N., Rosa, R., Stanaway, R., Oa, J., Nidkombu, E., Kwazi, J., 2014. Continental breakup and UHP rock exhumation in action: GPS results from the Woodlark Rift, Papua New Guinea. Geochem. Geophys. Geosystems 15, 4267–4290. https://doi.org/10.1002/2014GC005458

Wallace, L.M., Stevens, C., Silver, E., McCaffrey, R., Loratung, W., Hasiata, S., Stanaway, R., Curley, R., Rosa, R., Taugaloidi, J., 2004. GPS and seismological constraints on active tectonics and arc-continent collision in Papua New Guinea: Implications for mechanics of microplate rotations in a plate boundary zone. J. Geophys. Res. Solid Earth 109, 1–16. https://doi.org/10.1029/2003JB002481

Webb, L.E., Baldwin, S.L., Fitzgerald, P.G., 2014. The Early-Middle Miocene subduction complex of the Louisiade Archipelago, southern margin of the Woodlark Rift. Geochem. Geophys. Geosystems 15, 4024–4046. https://doi.org/10.1002/2014GC005500

Webb, L.E., Baldwin, S.L., Little, T.A., Fitzgerald, P.G., 2008. Can microplate rotation drive subduction inversion? Geology 36, 823–826. https://doi.org/10.1130/G25134A.1

Whattam, S.A., 2009. Arc-continent collisional orogenesis in the SW Pacific and the nature, source and correlation of emplaced ophiolitic nappe components. Lithos 113, 88–114. https://doi.org/10.1016/j.lithos.2008.11.009

Williams, I.S., Claesson, S., 1987. Isotopic evidence for the Precambrian provenance and Caledonian metamorphism of high grade paragneisses from the Seve Nappes, Scandinavian Caledonides. Contrib. Mineral. Petrol. 97, 205–217. https://doi.org/10.1007/BF00371240

Worthing, M.A., Crawford, A.J., 1996. The igneous geochemistry and tectonic setting of metabasites from the emo metamorphics, Papua New Guinea; A record of the evolution and destruction of a backarc basin. Mineral. Petrol. 58, 79–100. https://doi.org/10.1007/BF01165765

Zahirovic, S., Matthews, K.J., Flament, N., Müller, R.D., Hill, K.C., Seton, M., Gurnis, M., 2016. Tectonic evolution and deep mantle structure of the eastern Tethys since the latest Jurassic. Earth-Sci. Rev. 162, 293–337. https://doi.org/10.1016/j.earscirev.2016.09.005

Zirakparvar, N.A., Baldwin, S.L., Vervoort, J.D., 2013. The origin and geochemical evolution of the Woodlark Rift of Papua New Guinea. Gondwana Res. 23, 931–943. https://doi.org/10.1016/j.gr.2012.06.013

Highlights:

- The Goropu Metabasalt was erupted in the Late Cretaceous; the Yau Igneous Complex intruding those oceanic MORB basalts are Paleocene in age.
- Syn-extensional granitoids intruding the footwall of the Suckling-Dayman metamorphic core complex are late Pliocene to early Pleistocene in age.
- Xenocrystic zircons in the Plio-Pleistocene granitoids indicate an underlying Cretaceous-aged continental basement.
- Extensional reactivation of the Mai'iu Fault had commenced by ~3.7 Ma.